REPORT 972

THE EFFECT OF TORSIONAL FLEXIBILITY ON THE ROLLING CHARACTERISTICS AT SUPERSONIC SPEEDS OF TAPERED UNSWEPT WINGS

By Warren A. Tucker and Robert L. Nelson

SUMMARY

An analysis is presented of the effect of torsional flexibility on the rolling characteristics at supersonic speeds of tapered unswept wings with partial-span constant-percent-chord ailerons extending inboard from the wing tip. The geometric variables considered are aspect ratio, taper ratio, aileron span, and aileron chord.

The shape of the wing-torsional-stiffness curve is assumed and the twisting moment is considered to result solely from the pressure distribution caused by aileron deflection, so that the necessity of using a successive-approximation method is avoided.

Because of the complexity of the equations resulting from the analysis, numerical calculations from the equations are presented in a series of figures. A computational form is provided to be used in conjunction with these figures so that calculations can be made without reference to the analysis.

INTRODUCTION

In reference 1 an analysis was presented of the effect of torsional flexibility on the rolling characteristics at supersonic speeds of rectangular wing-aileron combinations. The present report deals with the more general case of linearly tapered wings having straight midchord lines and incorporating partial-span constant-percent-chord ailerons extending inboard from the wing tip (fig. 1) and may thus be considered a companion piece to reference 2, which gives an analysis of the rolling characteristics of this class of wings at subsonic speeds.

The necessity of using successive approximations is avoided by assuming, as in reference 1, that the principal twisting moment is contributed by the loads arising from aileron deflection. The various aerodynamic forces and moments are calculated by methods based mainly on the linearized equations for three-dimensional supersonic flow.

The geometric variables considered are aspect ratio, taper ratio, aileron span, and aileron chord. The torsional stiffness of the wing is assumed to vary inversely with the cube of the distance outboard from the wing center line.

Because of the length of the equations for the various quantities appearing in the analysis, numerical calculations have been made for ranges of the variables considered. The results can be used, together with a computational form that is provided, to make calculations without reference to the details of the analysis.

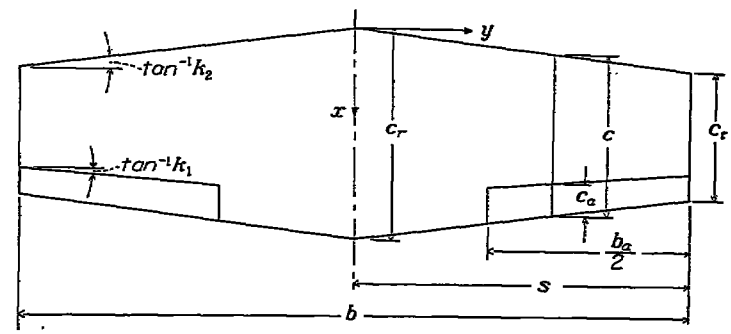

FIGURE 1.—The configuration investigated. $\frac{c_a}{c}$=Constant.

SYMBOLS

A	aspect ratio $\left(A=\frac{b^2}{S}=\frac{2b}{c_r(1+\lambda)}\right)$
b	wing span
b_a	total span of two ailerons
c	wing chord at spanwise station y
c_a	aileron chord at spanwise station y
c_r	root chord
c_t	tip chord
λ	taper ratio (c_t/c_r)
k_1	slope of hinge line (see fig. 1) $\left(\left(1-\frac{2c_a}{c}\right)\frac{2}{A}\frac{1-\lambda}{1+\lambda}\right)$
k_2	slope of leading edge (see fig. 1) $\left(\frac{2}{A}\frac{1-\lambda}{1+\lambda}\right)$
S	wing area $\left(\frac{bc_r}{2}(1+\lambda)\right)$
s	semispan $(b/2)$
x, y	coordinate axes (see fig. 1)
$\eta=\frac{y}{s}$	
M	free-stream Mach number
M_N	free-stream Mach number component normal to hinge line
$\beta\equiv\sqrt{M^2-1}$	
$\zeta=\frac{k_1}{\beta}$	
$\xi=\frac{k_2}{\beta}$	

γ	ratio of specific heat at constant pressure to specific heat at constant volume (1.40 for air)
p_o	free-stream static pressure
q	free-stream dynamic pressure $\left(\frac{\gamma}{2}p_oM^2\right)$
P	lifting pressure
C_p	lifting-pressure coefficient (P/q)
C_{p_∞}	additional two-dimensional lifting-pressure coefficient due to aileron deflection $\left(\frac{4\delta}{\beta\sqrt{1-\zeta^2}}\right)$
δ	deflection of one aileron, measured in plane perpendicular to wing and parallel to free stream, positive when right aileron is deflected up
θ	angle of twist at any spanwise station, positive when leading edge of right wing moves up
θ_r	angle of twist at reference station (midspan of aileron)
$pb/2V$	wing-tip helix angle
p	rolling angular velocity, positive when right wing moves down
a	constant of proportionality for parabolic twist distribution
w	vertical disturbance velocity
V	free-stream velocity
L	rolling moment, positive when tending to depress right wing
C_l	rolling-moment coefficient (L/qSb)
C_{l_δ}	rolling-moment-effectiveness coefficient for two ailerons $(\partial C_l/\partial\delta)$
C_{l_p}	damping-in-roll coefficient $\left(\partial C_l/\partial\frac{pb}{2V}\right)$
$C_{l_{\theta_r}}$	rolling-moment-loss coefficient $(\partial C_l/\partial\theta_r)$
T	aerodynamic twisting moment at any spanwise station $\left(\int_y^s m\,dy\right)$
$T'=T\frac{2\beta}{C_{p_\infty}qc_t^3}$	
m	pitching moment about midchord at any spanwise station
GJ	torsional-stiffness parameter $\left(\frac{T}{d\theta/dy}\right)$
m_θ	torsional-stiffness parameter (T/θ)
m_{θ_r}	torsional-stiffness parameter at reference station (midspan of aileron)
k	constant of proportionality for stiffness distribution
F	trailing-edge-angle reduction factor
ϕ	included trailing-edge angle measured parallel to free stream
ϕ_N	included trailing-edge angle measured normal to hinge line

Subscript:

R	rigid
0	sea level
1, 2, 3, 4	indicate various regions of the wing
a, b, c	indicate various stations

All angles are in radians, unless otherwise specified.

ANALYSIS

GENERAL

In a steady roll, the resultant rolling moment acting on a wing of any plan form is zero. This statement can be written in equation form as:

$$\beta C_{l_\delta}\delta+\beta C_{l_p}\frac{pb}{2V}+\beta C_{l_{\theta_r}}\theta_r=0 \tag{1}$$

Equation (1) can be solved either for the rate of roll per unit aileron deflection or for the ratio of the rate of roll of a flexible wing to the rate of roll of a perfectly rigid wing $(\theta_r=0)$ for a given aileron deflection. The following equations are obtained:

$$\frac{pb/2V}{\delta}=\frac{\beta C_{l_\delta}+\beta C_{l_{\theta_r}}\frac{\theta_r}{\delta}}{-\beta C_{l_p}} \tag{2}$$

$$\frac{pb/2V}{(pb/2V)_R}=1-\frac{-\beta C_{l_{\theta_r}}}{\beta C_{l_\delta}}\frac{\theta_r}{\delta} \tag{3}$$

The problem now becomes one of finding expressions for the quantities βC_{l_δ}, βC_{l_p}, $\beta C_{l_{\theta_r}}$, and θ_r/δ for the class of wing-aileron combination considered; the rest of the analysis is concerned with this problem.

A knowledge of the twist along the span is needed for the determination of $\beta C_{l_{\theta_r}}$ and θ_r/δ; this requirement in turn necessitates finding the aerodynamic twisting moment at any spanwise station. In order to evaluate the aerodynamic twisting moment the following assumptions are made:

(1) The elastic axis and the center of pressure at any spanwise station of the loads resulting from rolling and from twist lie very near the midchord line. This assumption allows the twisting moments resulting from rolling and from twist to be neglected.

(2) The aerodynamic twisting moment results solely from the loads caused by aileron deflection. This assumption is a direct result of the first one.

(3) The loads caused by aileron deflection, wing twist, and rolling are mutually independent. This assumption corresponds to the familiar superposition principle of linearized theory.

(4) The aileron does not twist with respect to the wing.

An important result of making these assumptions is the elimination of any necessity for using a method of successive approximations.

The main part of the analysis follows: First, the pertinent

pressure distributions are discussed; next, the method of finding the twist along the span is outlined; and last, the results for the various quantities are given. Since the mathematics involved in each step is lengthy, no attempt is made to give all the details. Those readers whose primary interest is in the application of the results are advised to turn to the section entitled "Computational Procedure and Discussion" and to table I.

PRESSURE DISTRIBUTIONS

Three pressure distributions are necessary in order to determine βC_{l_δ}, βC_{l_p}, and $\beta C_{l_{\theta_r}}$. These pressure distributions are, respectively, that due to aileron deflection, that due to a wing twist increasing linearly with distance along the span (corresponding to a rolling wing), and that due to a wing twist increasing with the square of the distance along the span (the reason for using a parabolic twist is discussed in the section entitled "Twist ratio"). Each pressure distribution can be found by use of the methods of references 3 and 4 if appropriate source-sink distributions are used to represent in one case the deflected aileron and in the other cases the twisted wing. The details of the derivations are not given; an illustration of the use of the method for finding the pressure distribution over a twisted wing can be found in the appendix of reference 1.

The equations for the pressure distribution due to aileron deflection are

$$\left.\begin{aligned}
\frac{C_{p_1}}{F}&=\frac{4\delta}{\pi\beta\sqrt{1-\zeta^2}}\left(\frac{\pi}{2}+\sin^{-1}\frac{\zeta+\frac{\beta v}{u}}{1+\frac{\zeta\beta v}{u}}\right)\\
\frac{C_{p_2}}{F}&=\frac{4\delta}{\beta\sqrt{1-\zeta^2}}\\
\frac{C_{p_3}}{F}&=\frac{8\delta}{\pi\beta\sqrt{1-\zeta^2}}\cos^{-1}\sqrt{\frac{1+\frac{\beta v}{u}}{1+\frac{\zeta\beta v}{u}}}
\end{aligned}\right\}\tag{4}$$

for the regions indicated in sketch 1.

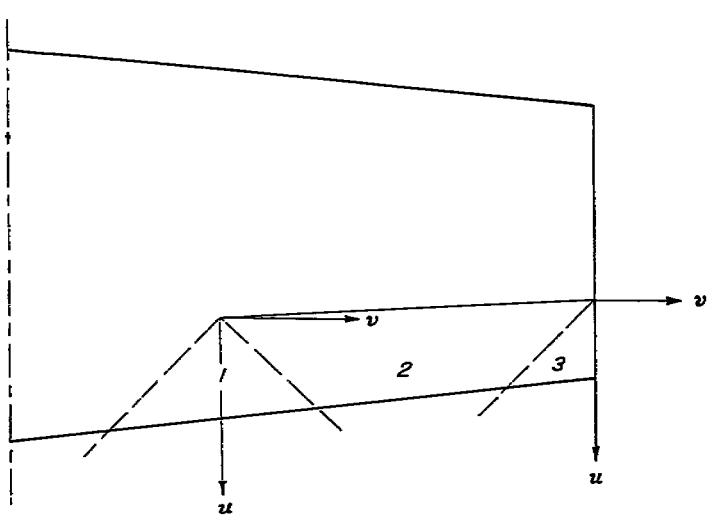

Sketch 1

The equations for the pressure distribution due to a wing twist increasing linearly with distance along the span ($w=py$) are

$$\left.\begin{aligned}
C_{p_1}&=\frac{8py/V}{\pi\beta(1-\xi^2)^{3/2}}\left(\cos^{-1}\xi\sqrt{\frac{1-\nu_1^2}{1-\xi^2\nu_1^2}}-\frac{\xi}{\nu_1}\cos^{-1}\sqrt{\frac{1-\nu_1^2}{1-\xi^2\nu_1^2}}\right)\\
C_{p_2}&=\frac{4py/V}{\beta(1-\xi^2)^{3/2}}\left(1-\frac{\xi}{\nu_1}\right)\\
C_{p_3}&=-\frac{\frac{8p(s-y)}{V}}{\pi\beta(1-\xi^2)^{3/2}}\left[\left(1+\frac{\xi}{\nu_2}\right)\cos^{-1}\sqrt{\frac{1-\nu_2}{1+\xi\nu_2}}+\right.\\
&\qquad\left.\sqrt{(1+\xi)\left(\frac{1}{\nu_2}-1\right)}\right]+\frac{8ps/V}{\pi\beta(1-\xi^2)^{1/2}}\cos^{-1}\sqrt{\frac{1-\nu_2}{1+\xi\nu_2}}
\end{aligned}\right\}\tag{5}$$

where

$$\nu_1=\frac{\beta y}{x}$$

$$\nu_2=\frac{\beta(s-y)}{x-k_2 s}$$

and the regions are indicated in sketch 2.

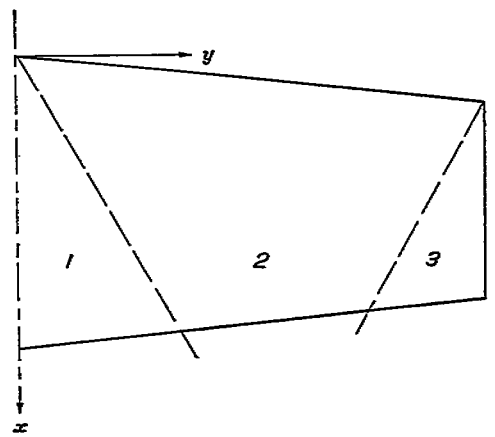

Sketch 2

The equations for the pressure distribution due to a wing twist increasing with the square of the distance along the span ($w=ay^2$) are

$$\left.\begin{aligned}
C_{p_1}&=\frac{4ay^2/V}{\pi\beta(1-\xi^2)^{5/2}}\left[\left(2+\xi^2+\frac{2\xi^2+1}{\nu_1^2}\right)\cos^{-1}\sqrt{\frac{1-\nu_1^2}{1-\xi^2\nu_1^2}}-\right.\\
&\qquad\left.\frac{6\xi}{\nu_1}\cos^{-1}\xi\sqrt{\frac{1-\nu_1^2}{1-\xi^2\nu_1^2}}\right]\\
C_{p_2}&=\frac{2ay^2/V}{\beta(1-\xi^2)^{5/2}}\left(2+\xi^2-\frac{6\xi}{\nu_1}+\frac{2\xi^2+1}{\nu_1^2}\right)\\
C_{p_3}&=\frac{\frac{4a(s-y)^2}{V}}{\pi\beta(1-\xi^2)^{5/2}}\left[\left(2+\xi^2+\frac{6\xi}{\nu_2}+\frac{2\xi^2+1}{\nu_2^2}\right)\cos^{-1}\sqrt{\frac{1-\nu_2}{1+\xi\nu_2}}+\right.\\
&\qquad\left.\sqrt{1+\xi}\left(2-\xi+\frac{4\xi+1}{\nu_2}\right)\sqrt{1-\nu_2}\right]-\\
&\qquad\frac{\frac{16as(s-y)}{V}}{\pi\beta(1-\xi^2)^{3/2}}\left[\left(1+\frac{\xi}{\nu_2}\right)\cos^{-1}\sqrt{\frac{1-\nu_2}{1+\xi\nu_2}}+\right.\\
&\qquad\left.\sqrt{(1+\xi)\left(\frac{1}{\nu_2}-1\right)}\right]+\frac{8as^2/V}{\pi\beta(1-\xi^2)^{1/2}}\cos^{-1}\sqrt{\frac{1-\nu_2}{1+\xi\nu_2}}
\end{aligned}\right\}\tag{6}$$

where ν_1 and ν_2 and the regions (sketch 2) are the same as for the wing with twist increasing linearly with distance along the span.

TWIST

Aerodynamic twisting moment.—The aerodynamic twisting moment T at any spanwise station y is simply the total moment acting outboard of the station. Thus,

$$T=\int_y^s m\,dy \tag{7}$$

where m, the pitching moment about the midchord line at any spanwise station, arises from the pressure distribution caused by aileron deflection and can be calculated from equations (4).

The resulting expressions for the aerodynamic twisting moment were extremely complicated. The twisting-moment distribution was therefore approximated by a series of straight lines as shown in figure 2, where the exact and approximate distributions for a particular configuration are compared for two values of β. The equations for T'_a, T'_b, and T'_c (see fig. 2) are as follows:

$$\left.\begin{aligned}
T'_a=&\frac{\left(\frac{c_a}{c}\right)^2\left(1-\frac{c_a}{c}\right)}{1-\xi}\left[1+\frac{2\frac{c_a}{c}\xi}{1-\xi}+\frac{4}{3}\xi^2\frac{\left(\frac{c_a}{c}\right)^2}{(1-\xi)^2}\right]+\frac{\frac{c_a}{c}\left(1-\frac{c_a}{c}\right)}{6\xi}-\frac{\sqrt{1-\zeta}}{6\xi\sqrt{1-\xi}}\frac{c_a}{c}\left[1-\frac{c_a}{c}+\frac{\frac{c_a}{c}\xi}{2(1-\xi)}\right]\\
T'_b=&-\frac{\sqrt{1-\zeta}}{6\xi\sqrt{1-\xi}}\frac{c_a}{c}\left[1-\frac{c_a}{c}+\frac{\frac{c_a}{c}\xi}{2(1-\xi)}\right]+\left(1+\frac{1-\lambda}{\lambda}\frac{b_a}{b}\right)^3\frac{\frac{c_a}{c}\left(1-\frac{c_a}{c}\right)}{6\xi}\frac{2}{\pi}\cos^{-1}\sqrt{\frac{1-\zeta}{2}}-\\
&\left(1+\frac{1-\lambda}{\lambda}\frac{b_a}{b}\right)^3\frac{\sqrt{1-\zeta^2}}{2\sqrt{1-\xi^2}}\left\{\frac{\frac{c_a}{c}\xi\left(1-2\frac{c_a}{c}\right)}{6(1-\xi^2)}\left[1+\left(\frac{c_a}{c}\right)^2\left(1-\frac{3+3\xi^2}{1-\xi^2}\right)\right]-\frac{\frac{c_a}{c}\left(1-\frac{c_a}{c}\right)}{6\xi(1-\xi^2)}\right\}\frac{2}{\pi}\cos^{-1}\xi-\\
&\left(1+\frac{1-\lambda}{\lambda}\frac{b_a}{b}\right)^3\frac{\frac{c_a}{c}\sqrt{1-\zeta^2}}{\pi(1-\xi^2)}\left[\frac{\left(\frac{c_a}{c}\right)^2\xi^2\left(1-2\frac{c_a}{c}\right)}{1-\xi^2}+\frac{1}{6}\frac{c_a}{c}\right]\\
T'_c=&-\left(1+\frac{1-\lambda}{\lambda}\frac{b_a}{b}\right)^3\frac{\sqrt{1-\zeta^2}}{\sqrt{1-\xi^2}}\left\{\frac{\frac{c_a}{c}\xi\left(1-2\frac{c_a}{c}\right)}{6(1-\xi^2)}\left[1+\left(\frac{c_a}{c}\right)^2\left(1-\frac{3+3\xi^2}{1-\xi^2}\right)\right]-\frac{\frac{c_a}{c}\left(1-\frac{c_a}{c}\right)}{6\xi(1-\xi^2)}\right\}-\\
&\frac{\sqrt{1-\zeta}}{6\xi\sqrt{1-\xi}}\frac{c_a}{c}\left[1-\frac{c_a}{c}+\frac{\frac{c_a}{c}\xi}{2(1-\xi)}\right]
\end{aligned}\right\} \tag{8}$$

The spanwise stations for T'_a, T'_b, and T'_c are given by the following equations:

$$\left.\begin{aligned}
\eta_a&=1-\frac{2\lambda}{1-\lambda}\frac{\xi}{1-\xi}\frac{c_a}{c}\\
\eta_b&=1-\frac{b_a}{b}\\
\eta_c&=1-\frac{2\lambda}{1-\lambda}\frac{\xi}{1-\xi}\frac{c_a}{c}-\frac{1-\zeta}{1-\xi}\frac{b_a}{b}
\end{aligned}\right\} \tag{9}$$

The straight-line approximations to the twisting-moment distribution (see fig. 2) are given by:

$$\left.\begin{aligned}
T'_1&=T'_c\\
T'_2&=T'_c+\frac{T'_c-T'_b}{\eta_b-\eta_c}(\eta_c-\eta)\\
T'_3&=T'_b+\frac{T'_b-T'_a}{\eta_a-\eta_b}(\eta_b-\eta)\\
T'_4&=T'_a+\frac{T'_a}{1-\eta_a}(\eta_a-\eta)
\end{aligned}\right\} \tag{10}$$

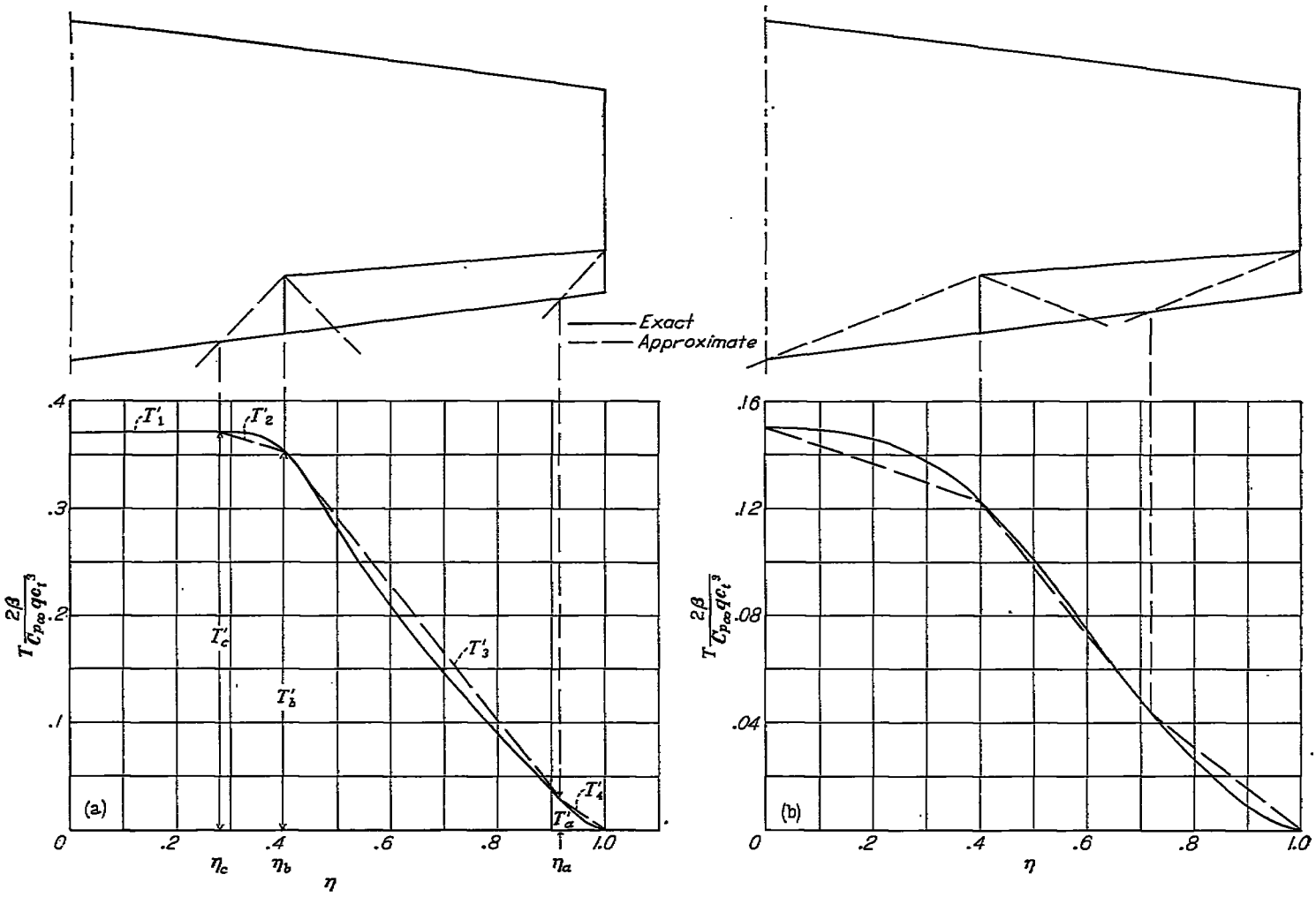

(a) $\beta=1.0$.

(b) $\beta=0.387$.

FIGURE 2.—Comparison of exact and approximate twisting-moment distribution for a particular configuration. $\lambda=0.6$; $A=4$; $\frac{b_a}{b}=0.6$; $\frac{c_a}{c}=0.2$; $T'=T\frac{2\beta}{C_{p_\infty}qc_t^3}$.

Twist at any spanwise station.—The twist θ at any spanwise station y can be calculated from the equation

$$\theta=\int_0^y \frac{d\theta}{dy}\,dy \tag{11}$$

where $d\theta/dy$ can be found from the definition of the torsional-stiffness parameter GJ, which is

$$GJ=\frac{T}{d\theta/dy} \tag{12}$$

and which is related to the torsional-stiffness parameter m_θ by the following equation:

$$\frac{1}{m_\theta}=\int_0^y \frac{dy}{GJ} \tag{13}$$

If the assumption is made that

$$\frac{1}{GJ}=ky^2 \tag{14a}$$

then

$$\frac{1}{m_\theta}=\frac{k}{3}y^3 \tag{14b}$$

This variation of torsional stiffness is known to be typical of many subsonic fighter airplanes (reference 2) and may be expected to approximate the stiffness distribution of airplanes or missiles designed for supersonic flight.

If equation (14a) is substituted in equation (12) and the result substituted in equation (11), then the twist is expressed as

$$\theta(y)=k\int_0^y y^2T(y)\,dy \tag{15}$$

If a change is made in the variable of integration by writing

$$\eta=\frac{y}{s}$$

and if T' is defined as

$$T'=T\,\frac{2\beta}{C_{p_\infty}qc_t^3} \tag{16}$$

then the expression for θ becomes

$$\theta(\eta)=\frac{C_{p_\infty}kqs^3c_t^3}{2\beta}\int_0^\eta \eta^2T'(\eta)\,d\eta \tag{17}$$

The integration must of course be carried out in steps, since T' is not defined continuously over the span.

The subscripts 1, 2, 3, and 4 may conveniently be used to indicate the regions designated by the same subscripts in figure 2. After substitution of the values of T' from equations (10) in equation (17) the twist equations become:

$$\theta_1 \frac{2\beta}{C_{p_\infty} kqs^3 c_t^3} = T'_c \frac{\eta^3}{3} \tag{18a}$$

$$\theta_2 \frac{2\beta}{C_{p_\infty} kqs^3 c_t^3} = \left(T'_c + \frac{T'_c - T'_b}{\eta_b - \eta_c}\eta_c\right)\frac{\eta^3}{3} - \left(\frac{T'_c - T'_b}{\eta_b - \eta_c}\right)\frac{\eta^4}{4} - \left(\frac{T'_c - T'_b}{\eta_b - \eta_c}\right)\frac{\eta_c^4}{12} \tag{18b}$$

$$\theta_3 \frac{2\beta}{C_{p_\infty} kqs^3 c_t^3} = \left(T'_b + \frac{T'_b - T'_a}{\eta_a - \eta_b}\eta_b\right)\frac{\eta^3}{3} - \left(\frac{T'_b - T'_a}{\eta_a - \eta_b}\right)\frac{\eta^4}{4} - \left(\frac{T'_b - T'_a}{\eta_a - \eta_b}\right)\frac{\eta_b^4}{12} + \left(\frac{T'_c - T'_b}{\eta_b - \eta_c}\right)\frac{\eta_b^4 - \eta_c^4}{12} \tag{18c}$$

$$\theta_4 \frac{2\beta}{C_{p_\infty} kqs^3 c_t^3} = \frac{T'_a}{1-\eta_a}\left(\frac{\eta^3}{3} - \frac{\eta^4}{4}\right) - \left(\frac{T'_b - T'_a}{\eta_a - \eta_b}\right)\frac{\eta_b^4}{12} + \left(\frac{T'_c - T'_b}{\eta_b - \eta_c}\right)\frac{\eta_b^4 - \eta_c^4}{12} + \frac{T'_b(1-\eta_a) - T'_a(1-\eta_b)}{(1-\eta_a)(\eta_a - \eta_b)}\frac{\eta_a^4}{12} \tag{18d}$$

Twist ratio.—For purposes of calculation, the twist may be expressed as the ratio of the twist θ at any station to the twist θ_r at a reference station taken at the midspan of the aileron $\left(\eta = 1 - \frac{1}{2}\frac{b_a}{b}\right)$. The twist is plotted in this manner in figure 3 for a particular configuration for two values of β. The exact results are based upon the approximate twisting-moment distribution shown in figure 2. Because θ/θ_r is not defined continuously over the span and because the defining expression is very complicated in each region, the subsequent evaluation of $\beta C_{l_{\theta_r}}$ is greatly simplified if a simple approximate equation for θ/θ_r, continuous over the span, is used. This approximation, which is also plotted in figure 3, is given by the following equation:

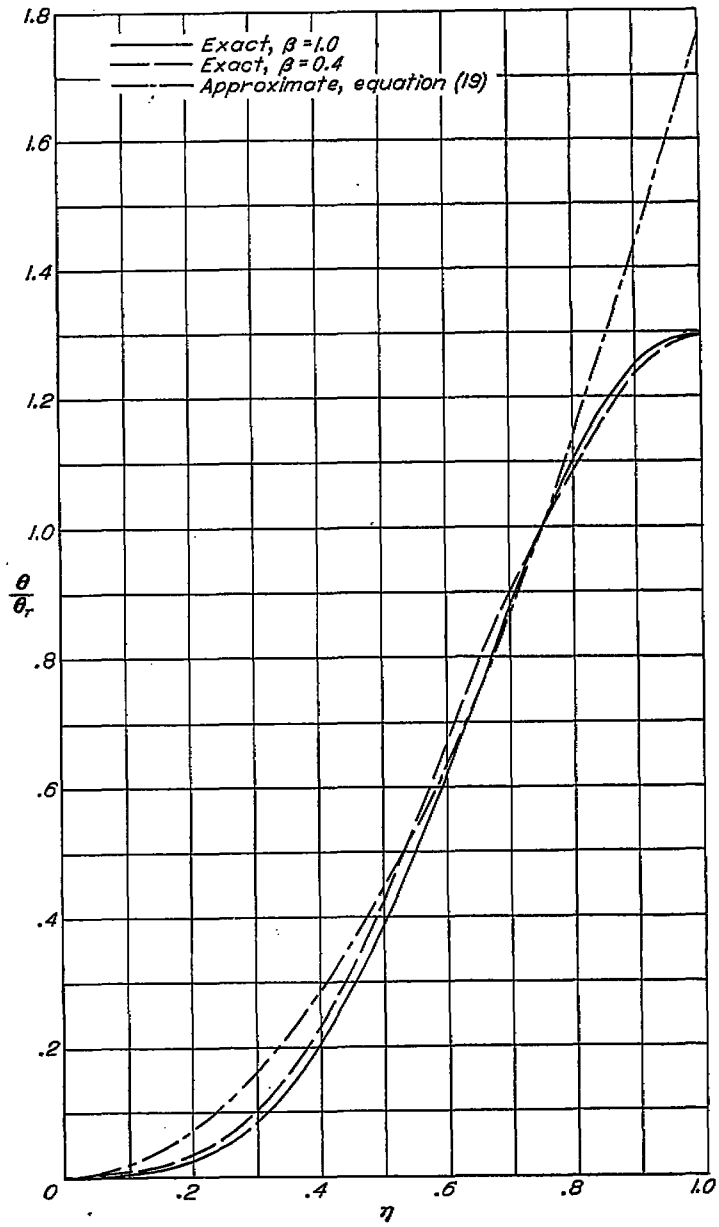

FIGURE 3.—Comparison of exact and approximate (equation (19)) twist distribution for a particular configuration. $\lambda = 0.5$; $A = 4$; $\frac{b_a}{b} = 0.5$; $\frac{c_a}{c} = 0.2$.

$$\frac{\theta}{\theta_r} = \frac{1}{\left(1 - \frac{1}{2}\frac{b_a}{b}\right)^2}\eta^2 \tag{19}$$

DERIVATIVES

Rolling-moment-effectiveness coefficient βC_{l_δ}.—The rolling-moment-effectiveness coefficient βC_{l_δ} is first found for a wing-aileron configuration of zero thickness (or zero trailing-edge angle) by suitable integration of the pressure distribution given by equations (4). A factor F is then applied to account for the effect of the trailing-edge angle.

The result obtained for the wing of zero thickness is given by the following equation:

$$\frac{\beta C_{l_\delta}}{F} = \frac{2}{1+\lambda}\frac{b_a}{b}\frac{c_a}{c}\left[2\lambda + (1-2\lambda)\frac{b_a}{b} - \frac{2}{3}(1-\lambda)\left(\frac{b_a}{b}\right)^2\right]\frac{1}{\sqrt{1-\zeta^2}} - \frac{2}{1-\lambda^2}\left(1 - \frac{b_a}{b}\right)\frac{c_a}{c}\left[\lambda + (1-\lambda)\frac{b_a}{b}\right]^2 \frac{1 - \xi^2 - \sqrt{(1-\zeta^2)(1-\xi^2)}}{\sqrt{1-\zeta^2}(1-\xi^2)} + \frac{2}{3(1-\lambda)(1-\lambda^2)}\frac{c_a}{c}\left[\lambda + (1-\lambda)\frac{b_a}{b}\right]^3 \frac{(1+\xi)(\xi-\zeta)^2 - (1-\xi^2)^2 + (1+\zeta\xi - 2\xi^2)\sqrt{(1-\zeta^2)(1-\xi^2)}}{\sqrt{1-\zeta^2}(1-\xi^2)^2} + \frac{2\lambda^2}{1-\lambda^2}\frac{c_a}{c}\frac{1 - \xi - \sqrt{(1-\zeta)(1-\xi)}}{\sqrt{1-\zeta^2}(1-\xi)} + \frac{\lambda^3}{3(1-\lambda)(1-\lambda^2)}\frac{c_a}{c}\frac{2(1-\xi)^2 - (2+\zeta-3\xi)\sqrt{(1-\zeta)(1-\xi)}}{\sqrt{1-\zeta^2}(1-\xi)^2} \tag{20}$$

The factor F that appears in equation (20) is discussed in the section entitled "Computational Procedure and Discussion."

Damping-in-roll coefficient βC_{l_p}.—The damping-in-roll coefficient βC_{l_p} is obtained by proper integration of the pressure distribution given by equations (5). The following result is obtained:

$$-\beta C_{l_p}=\frac{2}{\pi(1+\lambda)(1-\lambda)^3}\left[\frac{1-4\xi^2+8\xi^4}{3(1-\xi^2)^{7/2}}\cos^{-1}\xi+\frac{3\xi-10\xi^3-8\xi^5}{9(1-\xi^2)^3}\right]-\frac{\lambda^4}{3(1+\lambda)(1-\lambda)^3}\frac{2-6\xi+5\xi^2}{2(1-\xi)^3}-$$
$$\frac{4\lambda^3}{3(1+\lambda)(1-\lambda)^2}\frac{1-2\xi}{(1-\xi)^2}-\frac{2\lambda^2}{1-\lambda^2}\frac{1}{1-\xi} \tag{21}$$

Rolling-moment-loss coefficient $\beta C_{l_{\theta_r}}$.—The rolling-moment-loss coefficient $\beta C_{l_{\theta_r}}$ is obtained by suitable integration of the pressure distribution given by equations (6) by using

$$\frac{a}{V}=\frac{4}{b^2}\frac{\theta_r}{\left(1-\frac{1}{2}\frac{b_a}{b}\right)^2} \tag{22}$$

from equation (19), since $\theta=\frac{w}{V}$. The following result is obtained:

$$-\beta C_{l_{\theta_r}}\left(1-\frac{1}{2}\frac{b_a}{b}\right)^2=\frac{2}{15\pi(1-\lambda)^4(1+\lambda)}\left[\frac{\xi}{3(1-\xi^2)^4}(9-36\xi^2+100\xi^4+32\xi^6)+\frac{3-14\xi^2+24\xi^4-48\xi^6}{(1-\xi^2)^{9/2}}\cos^{-1}\xi\right]-$$
$$\frac{\lambda^5}{30(1-\lambda)^4(1+\lambda)}\frac{6-24\xi+35\xi^2-20\xi^3}{(1-\xi)^4}-\frac{\lambda^4}{6(1-\lambda)^3(1+\lambda)}\frac{6-18\xi+17\xi^2}{(1-\xi)^3}-$$
$$\frac{2\lambda^3}{(1-\lambda)^2(1+\lambda)}\frac{1-2\xi}{(1-\xi)^2}-\frac{2\lambda^2}{(1-\lambda)(1+\lambda)}\frac{1}{1-\xi} \tag{23}$$

Twist parameter θ_r/δ.—The twist parameter θ_r/δ can be evaluated from equations (18c) and (18d) for $1-\frac{1}{2}\frac{b_a}{b}$ less than or greater than η_a, respectively. In order to perform the evaluation, the value of C_{p_∞} is taken from equations (4) to be the following:

$$C_{p_\infty}=\frac{4\delta}{\beta\sqrt{1-\zeta^2}} \tag{24}$$

The use of this linearized-theory result is conservative. The value of k is found from equation (14b) to be the following:

$$k=\frac{24}{b^3 m_{\theta_r}\left(1-\frac{1}{2}\frac{b_a}{b}\right)^3} \tag{25}$$

The following equations are obtained for θ_r/δ:

For $1-\frac{1}{2}\frac{b_a}{b}<\eta_a$,

$$\frac{\theta_r}{\delta}=\frac{b^3\beta q}{m_{\theta_r}}\frac{6\lambda^3}{\left(1-\frac{1}{2}\frac{b_a}{b}\right)^3(1-\lambda)^3}\frac{\xi^3}{\sqrt{1-\zeta^2}}\left[\left(T'_b+\frac{T'_b-T'_a}{\eta_a-\eta_b}\eta_b\right)\frac{1}{3}\left(1-\frac{1}{2}\frac{b_a}{b}\right)^3-\frac{T'_b-T'_a}{\eta_a-\eta_b}\frac{1}{4}\left(1-\frac{1}{2}\frac{b_a}{b}\right)^4-\frac{T'_b-T'_a}{\eta_a-\eta_b}\frac{\eta_b^4}{12}+\frac{T'_c-T'_b}{\eta_b-\eta_c}\frac{\eta_b^4-\eta_c^4}{12}\right] \tag{26a}$$

and for $1-\frac{1}{2}\frac{b_a}{b}>\eta_a$,

$$\frac{\theta_r}{\delta}=\frac{b^3\beta q}{m_{\theta_r}}\frac{6\lambda^3}{\left(1-\frac{1}{2}\frac{b_a}{b}\right)^3(1-\lambda)^3}\frac{\xi^3}{\sqrt{1-\zeta^2}}\left[\frac{T'_a}{1-\eta_a}\frac{1}{3}\left(1-\frac{1}{2}\frac{b_a}{b}\right)^3-\frac{T'_a}{1-\eta_a}\frac{1}{4}\left(1-\frac{1}{2}\frac{b_a}{b}\right)^4-\frac{T'_b-T'_a}{\eta_a-\eta_b}\frac{\eta_b^4}{12}+\frac{T'_c-T'_b}{\eta_b-\eta_c}\frac{\eta_b^4-\eta_c^4}{12}+\right.$$
$$\left.\frac{T'_b(1-\eta_a)-T'_a(1-\eta_b)}{(1-\eta_a)(\eta_a-\eta_b)}\frac{\eta_a^4}{12}\right] \tag{26b}$$

COMPUTATIONAL PROCEDURE AND DISCUSSION

In order to simplify the solution of equations (2) and (3) a computational form has been prepared. This computational form, which is presented as table I, is practically self-explanatory and can be used without reference to the analysis. Figures 4 to 15 contain the necessary information to be entered in the table. Most of these figures present the results of numerical calculations made from equations (20), (21), (23), and (26); the variables ξ and ζ appearing in these equations have been replaced by the appropriate combinations of βA, λ, and c_a/c so that the figures contain these more familiar quantities. The curves for the rectangular wing ($\lambda=1.0$) were taken from reference 1. Although in principle these curves could have been obtained from the equations of the present report, the work involved in evaluating the many indeterminate forms arising when $\lambda=1.0$ made such a procedure impractical.

The factor F which appears in equation (20) is introduced to allow for the effect of the trailing-edge angle. This factor is the same one shown in figure 7 of reference 1 and was derived by using Busemann's second-order approximation for isentropic flow. For the purposes of the present report, the Mach number and trailing-edge angle must be taken normal to the aileron hinge line. The factor F is plotted in figure 10 against M_N, the Mach number component normal to the aileron hinge line, with ϕ_N, the included trailing-edge angle measured normal to the aileron hinge line, as the parameter. The relations between M_N and M and between ϕ_N and ϕ are given by the following equations:

$$M_N=\frac{M}{\sqrt{1+k_1^2}}$$

$$=\frac{M}{\sqrt{1+\left(1-2\frac{c_a}{c}\right)^2\left(\frac{2}{A}\frac{1-\lambda}{1+\lambda}\right)^2}} \tag{27}$$

$$\phi_N=2\tan^{-1}\left(\frac{1+k_1k_2}{\sqrt{1+k_1^2}}\tan\frac{\phi}{2}\right)$$

$$=2\tan^{-1}\left[\frac{1+\left(1-2\frac{c_a}{c}\right)\left(\frac{2}{A}\frac{1-\lambda}{1+\lambda}\right)^2}{\sqrt{1+\left(1-2\frac{c_a}{c}\right)^2\left(\frac{2}{A}\frac{1-\lambda}{1+\lambda}\right)^2}}\tan\frac{\phi}{2}\right] \tag{28}$$

For ailerons other than those having flat sides, the trailing-edge angle should be taken as the angle between straight lines drawn from the trailing edge to the airfoil surface at the hinge line. For βC_{l_δ} this procedure can be shown to give the correct value of F independent of the airfoil profile; however, this method of determining F for curved-profile control surfaces is not valid for trailing-edge-angle corrections to hinge moments.

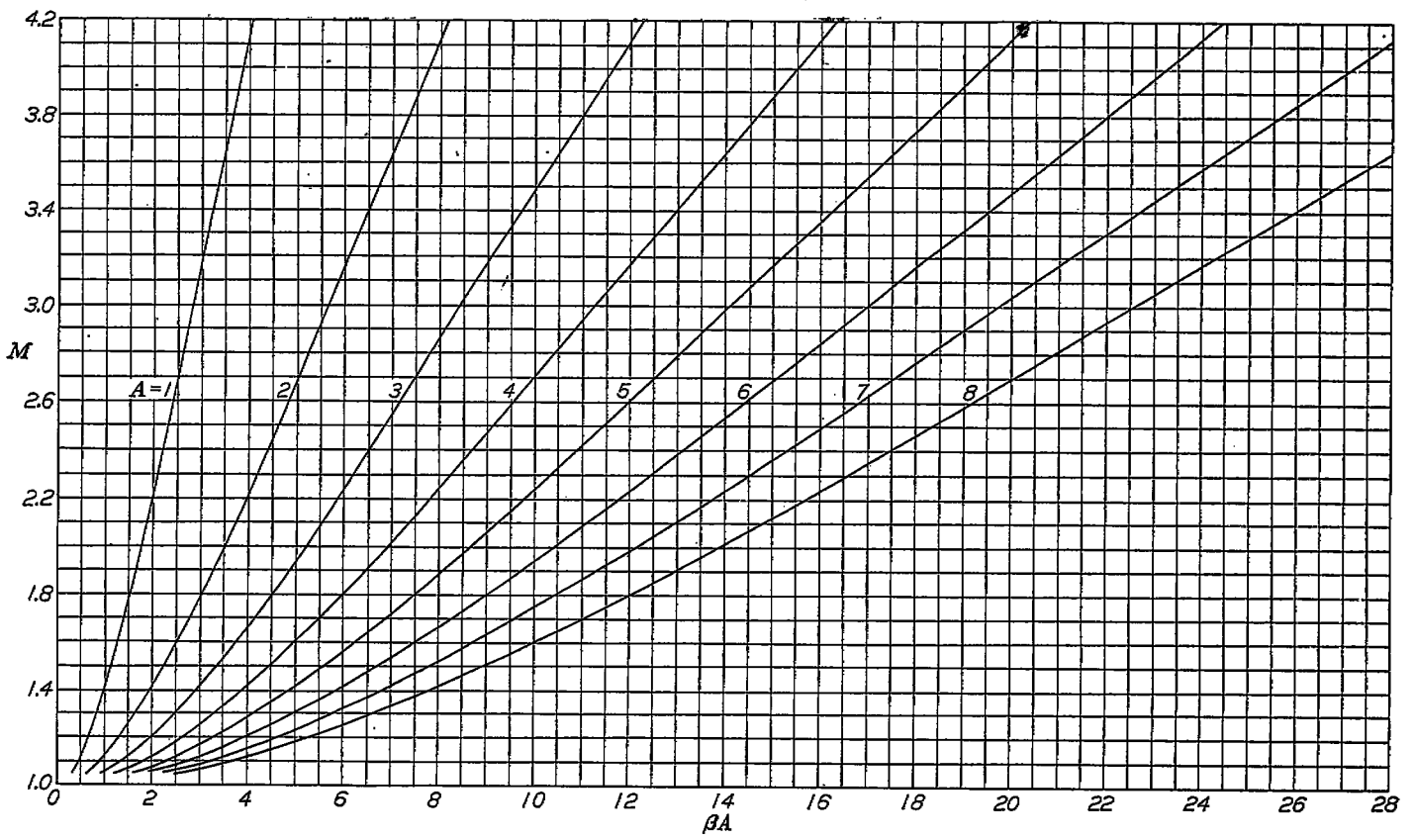

FIGURE 4.—Variation of M with βA.

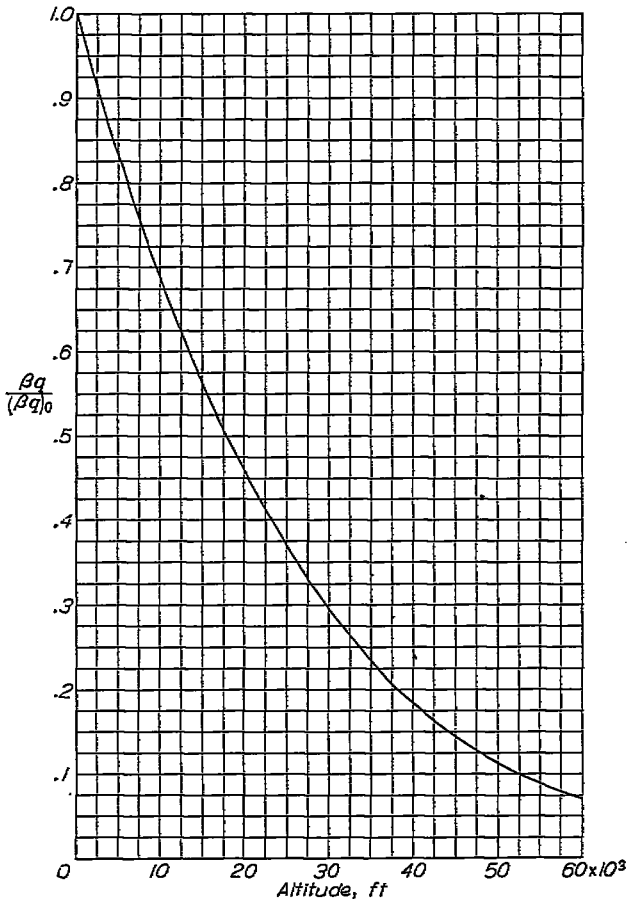

FIGURE 5.—Variation of dynamic-pressure ratio with altitude at constant Mach number.

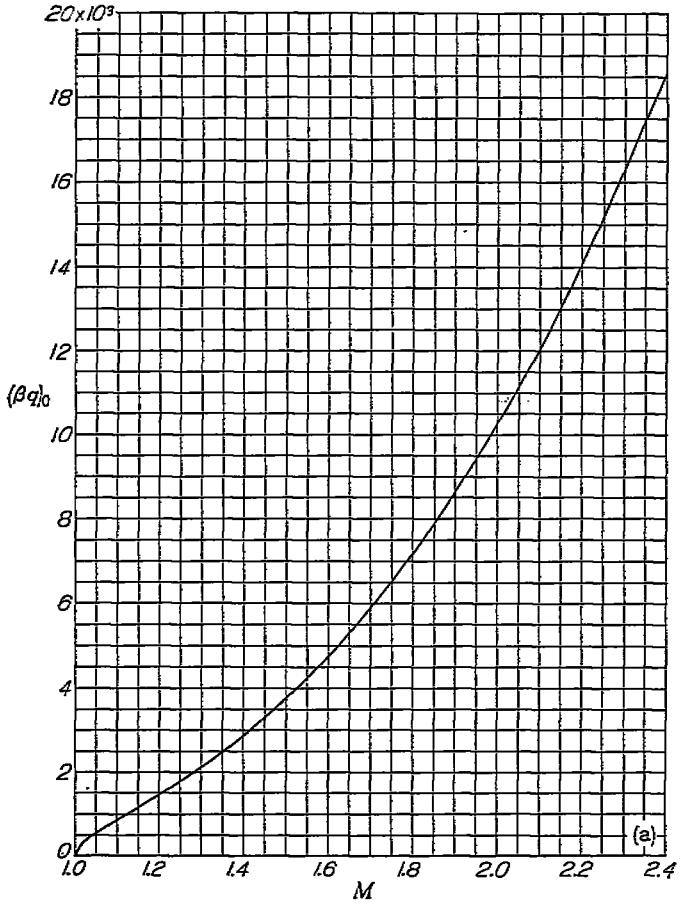

(a) $1.0 \leq M \leq 2.4$.

FIGURE 6.—Variation of $(\beta q)_0$ with M.

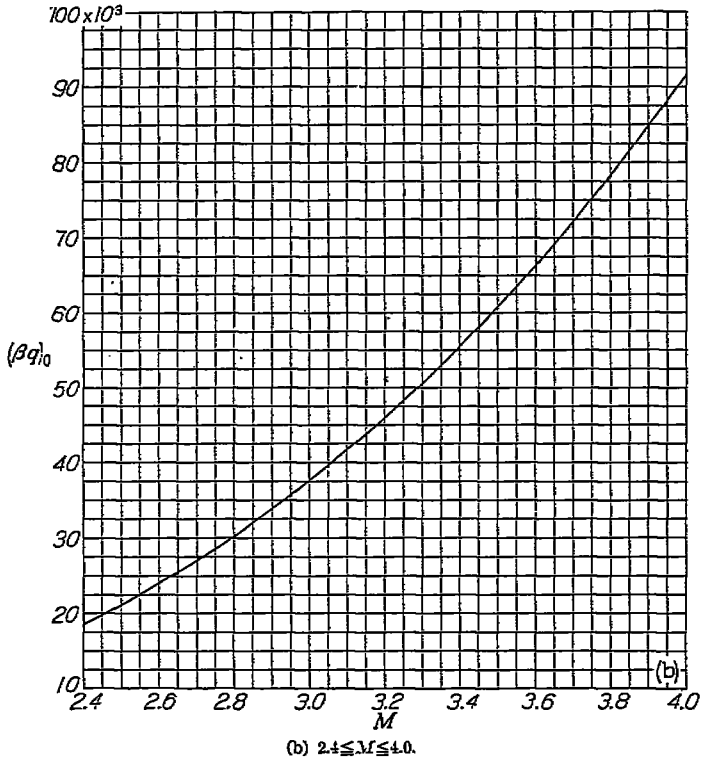

(b) $2.4 \leq M \leq 4.0$.

FIGURE 6.—Concluded.

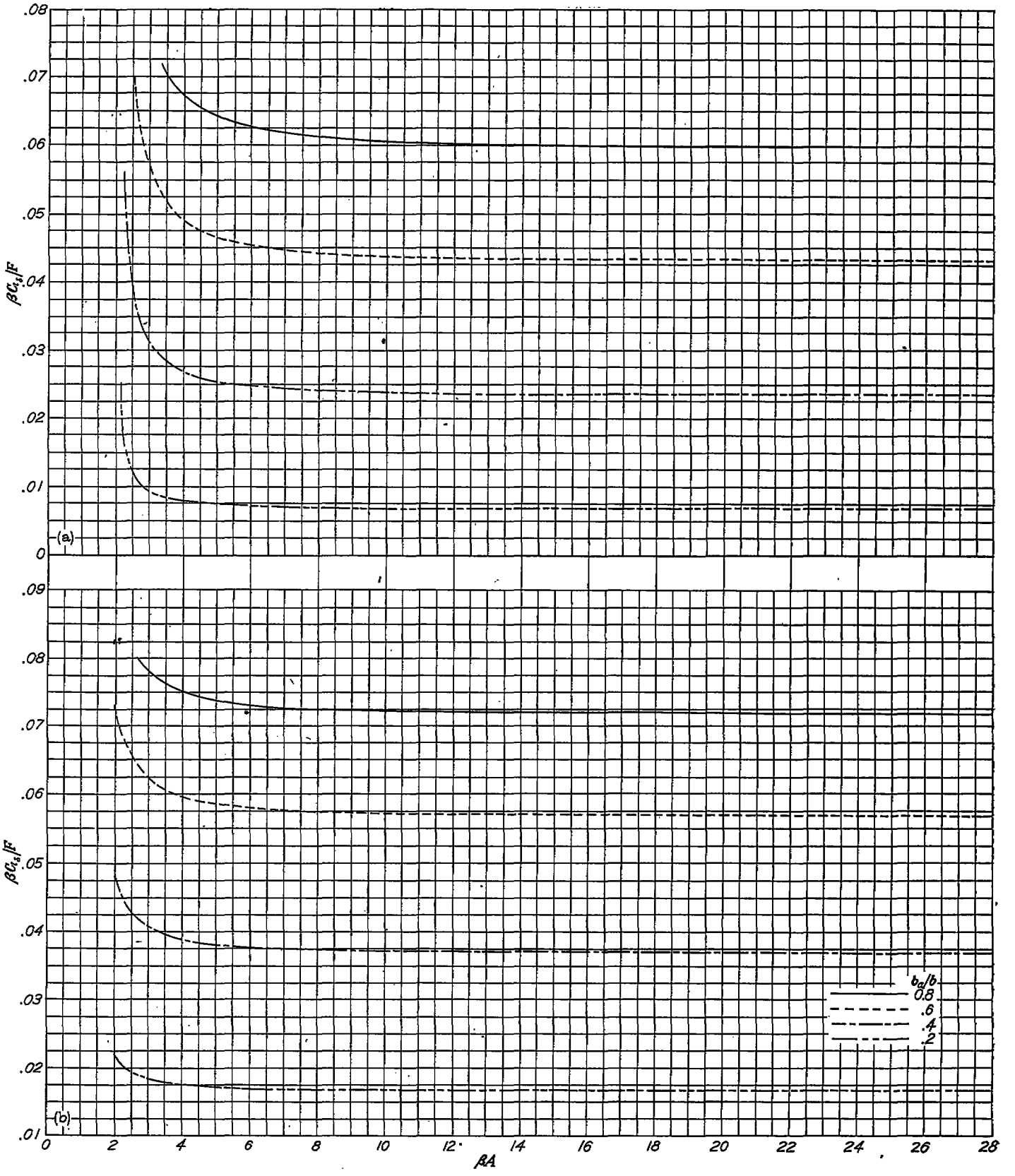

(a) $\lambda=0$.
(b) $\lambda=0.2$.

FIGURE 7.—Variation of rolling-moment-effectiveness coefficient with βA. $\frac{c_a}{c}=0.1$. (From equation (20).)

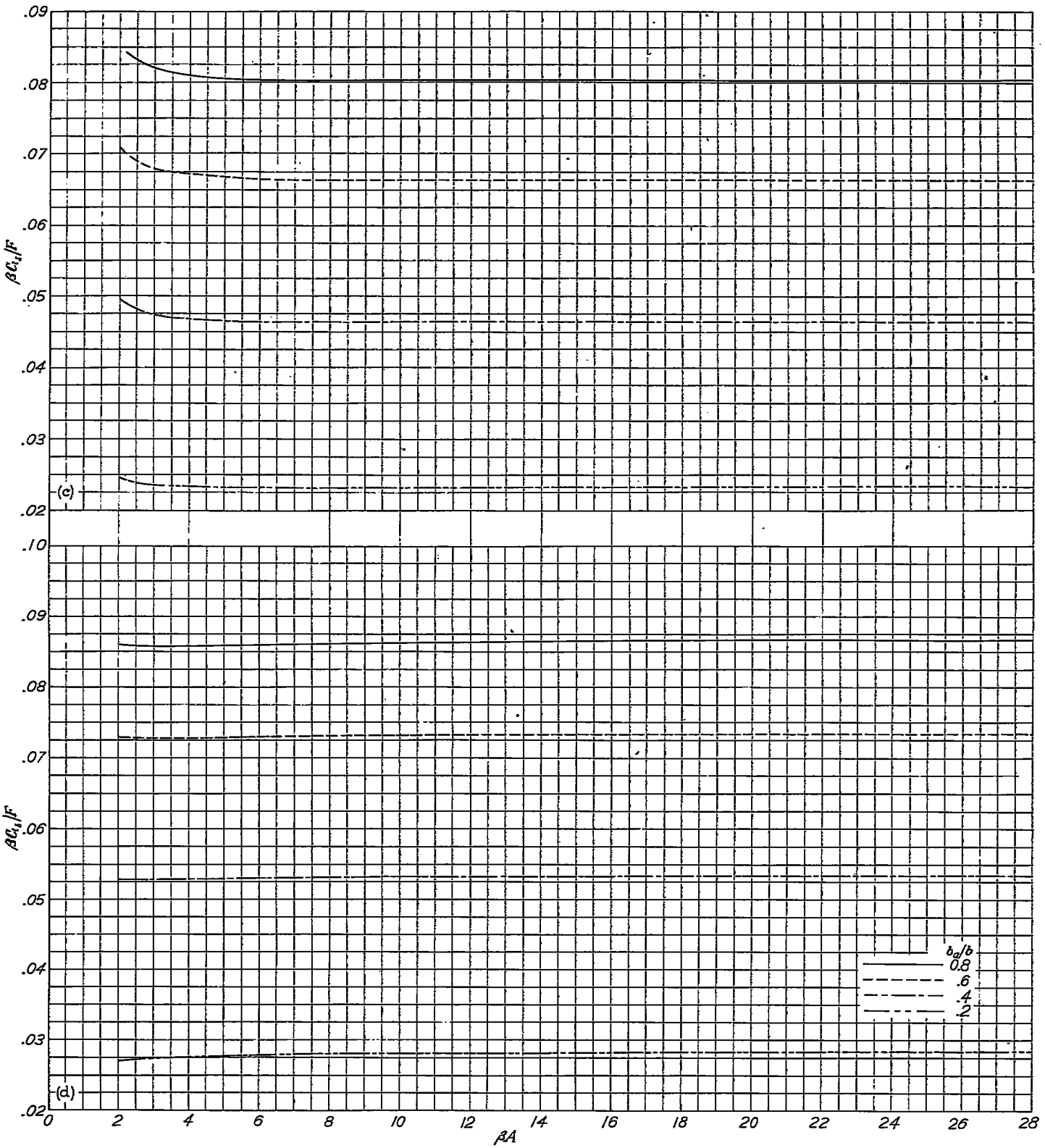

(c) $\lambda=0.4$.
(d) $\lambda=0.6$.

FIGURE 7.—Continued.

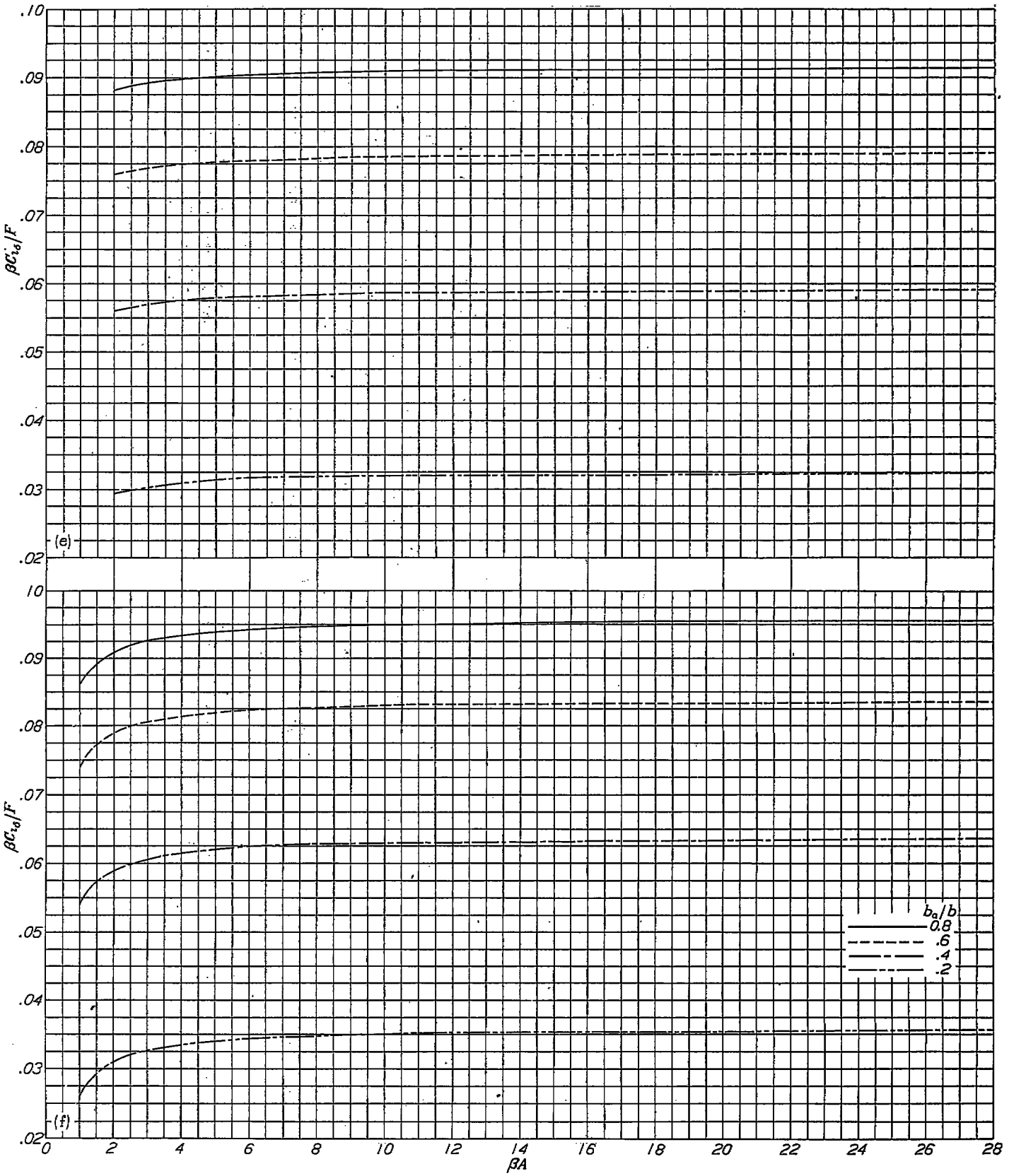

(e) $\lambda=0.8$.
(f) $\lambda=1.0$. (From reference 1.)

FIGURE 7.—Concluded.

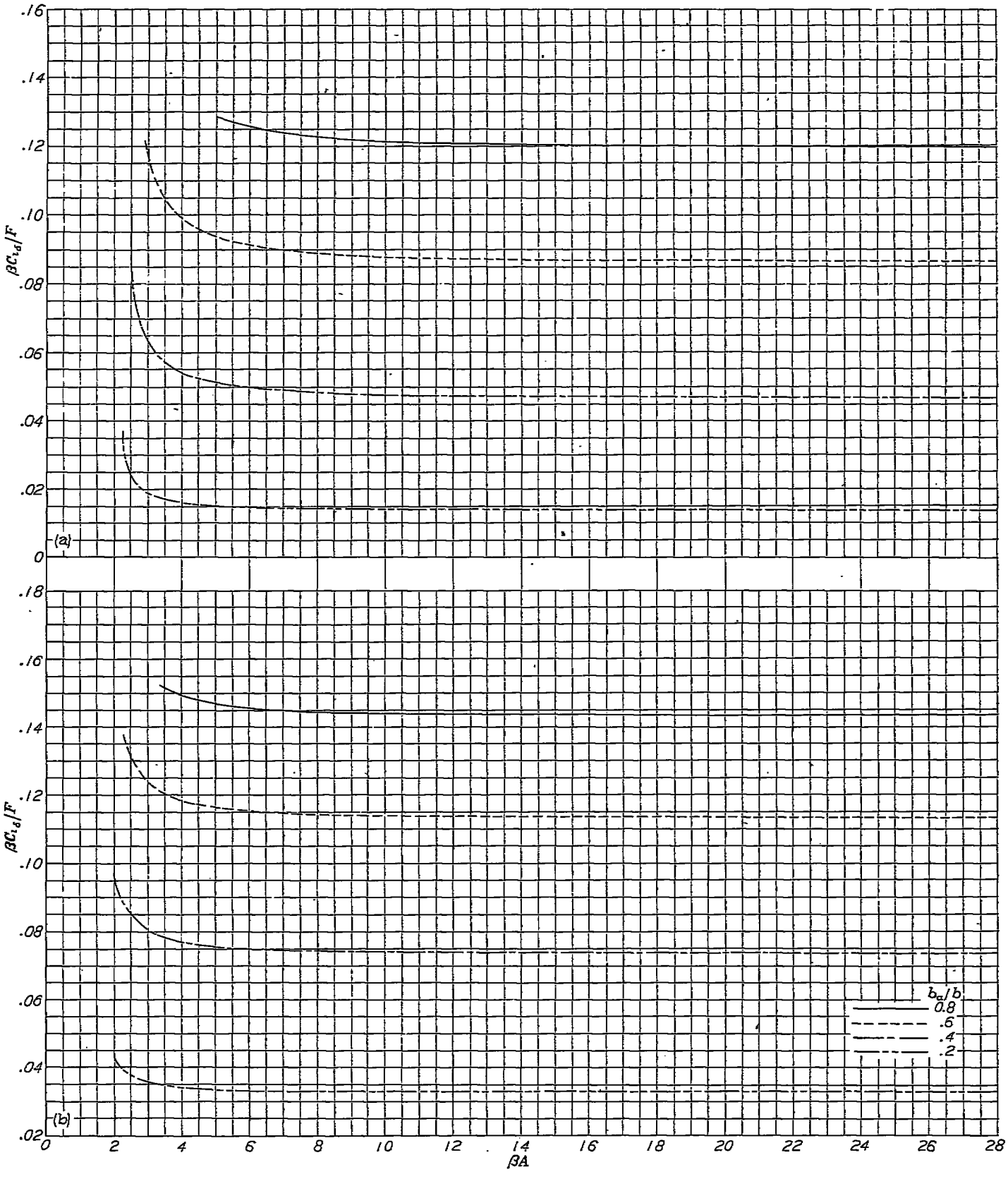

(a) $\lambda=0$.
(b) $\lambda=0.2$.

FIGURE 8.—Variation of rolling-moment-effectiveness coefficient with βA. $\frac{c_a}{c}=0.2$. (From equation (20).)

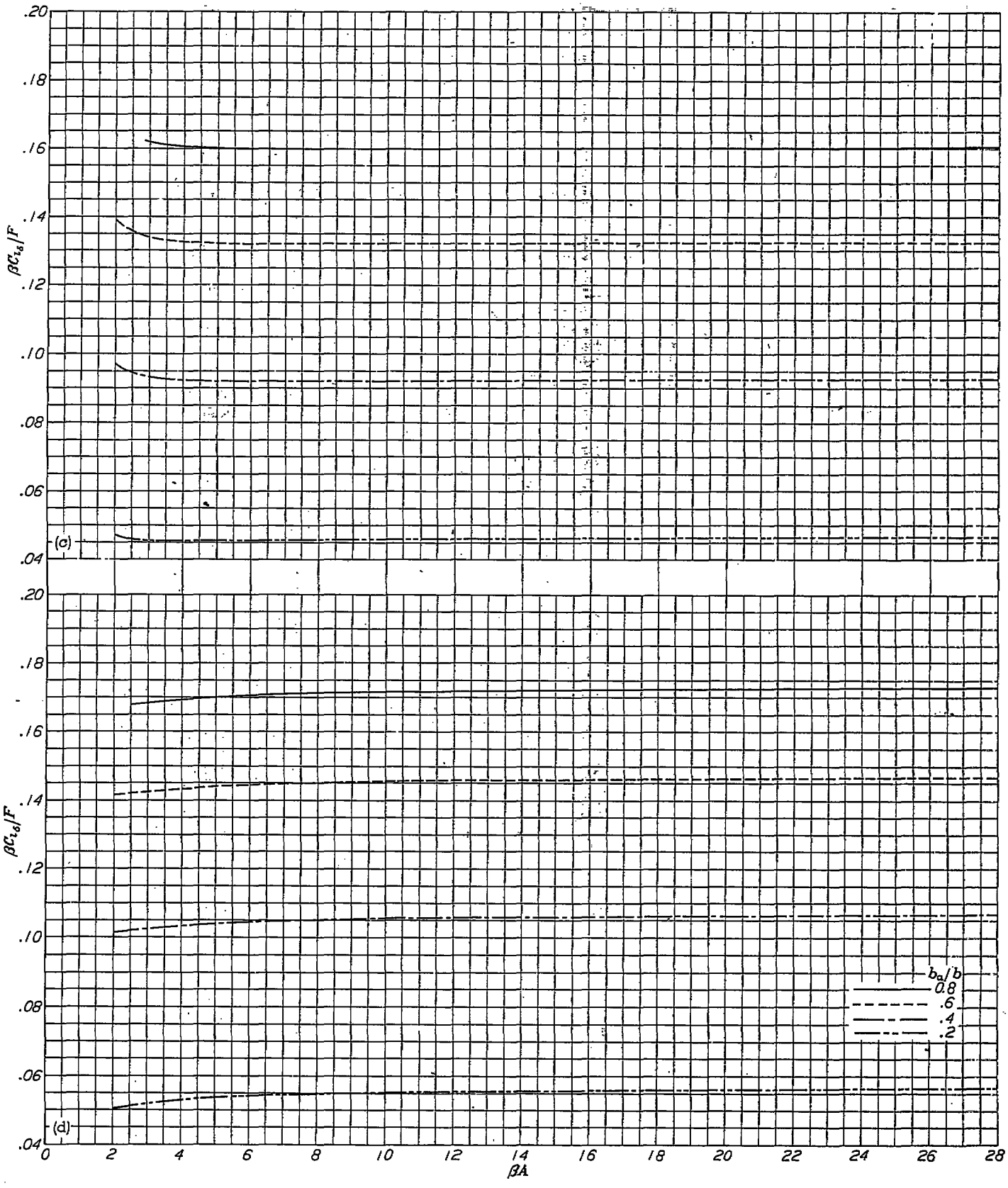

(c) $\lambda=0.4$.
(d) $\lambda=0.6$.

FIGURE 8.—Continued.

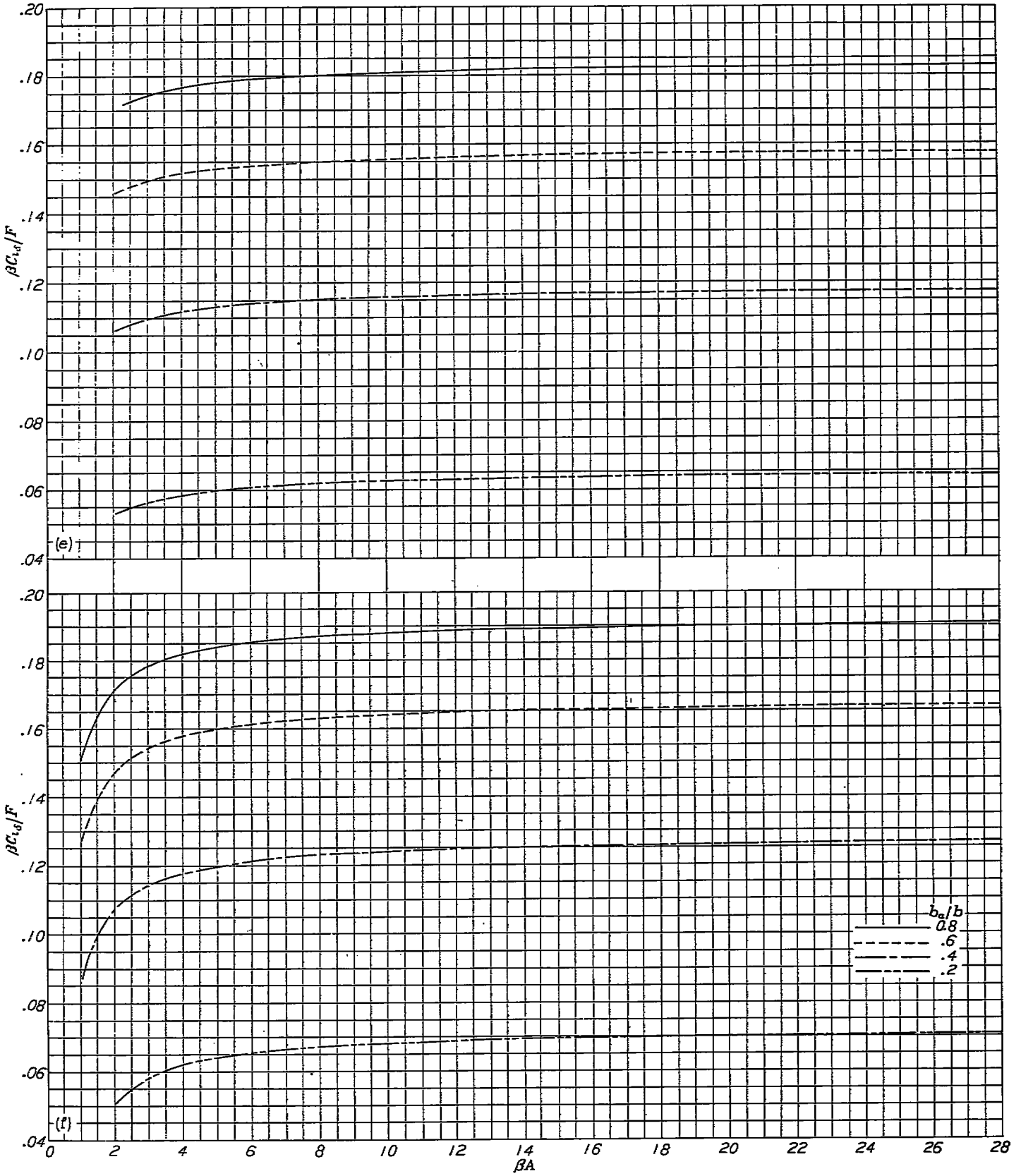

(e) $\lambda=0.8$.
(f) $\lambda=1.0$. (From reference 1.)

FIGURE 8.—Concluded.

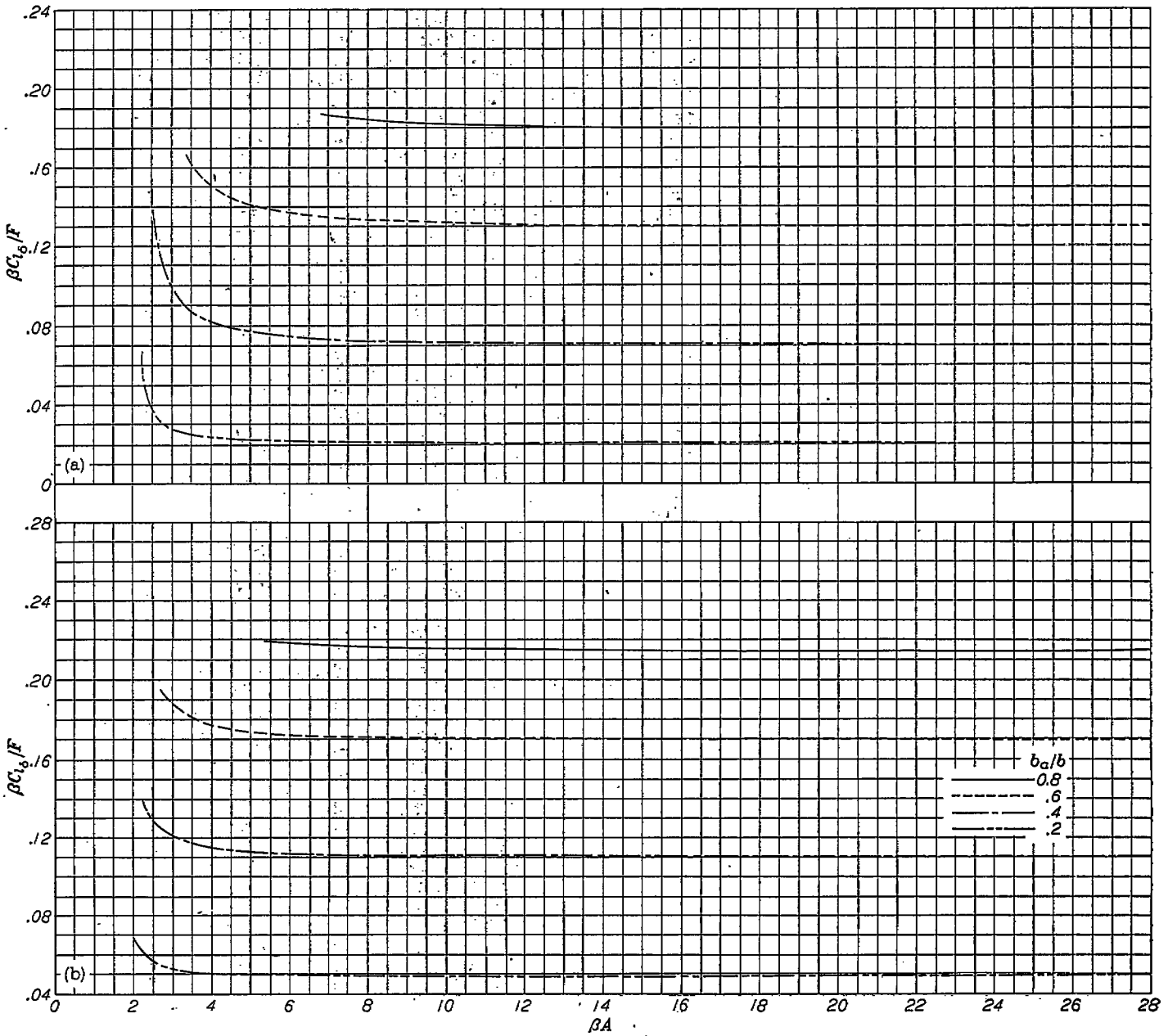

(a) $\lambda=0$.
(b) $\lambda=0.2$.

FIGURE 9.—Variation of rolling-moment-effectiveness coefficient with βA. $\frac{c_a}{c}=0.3$. (From equation (20).)

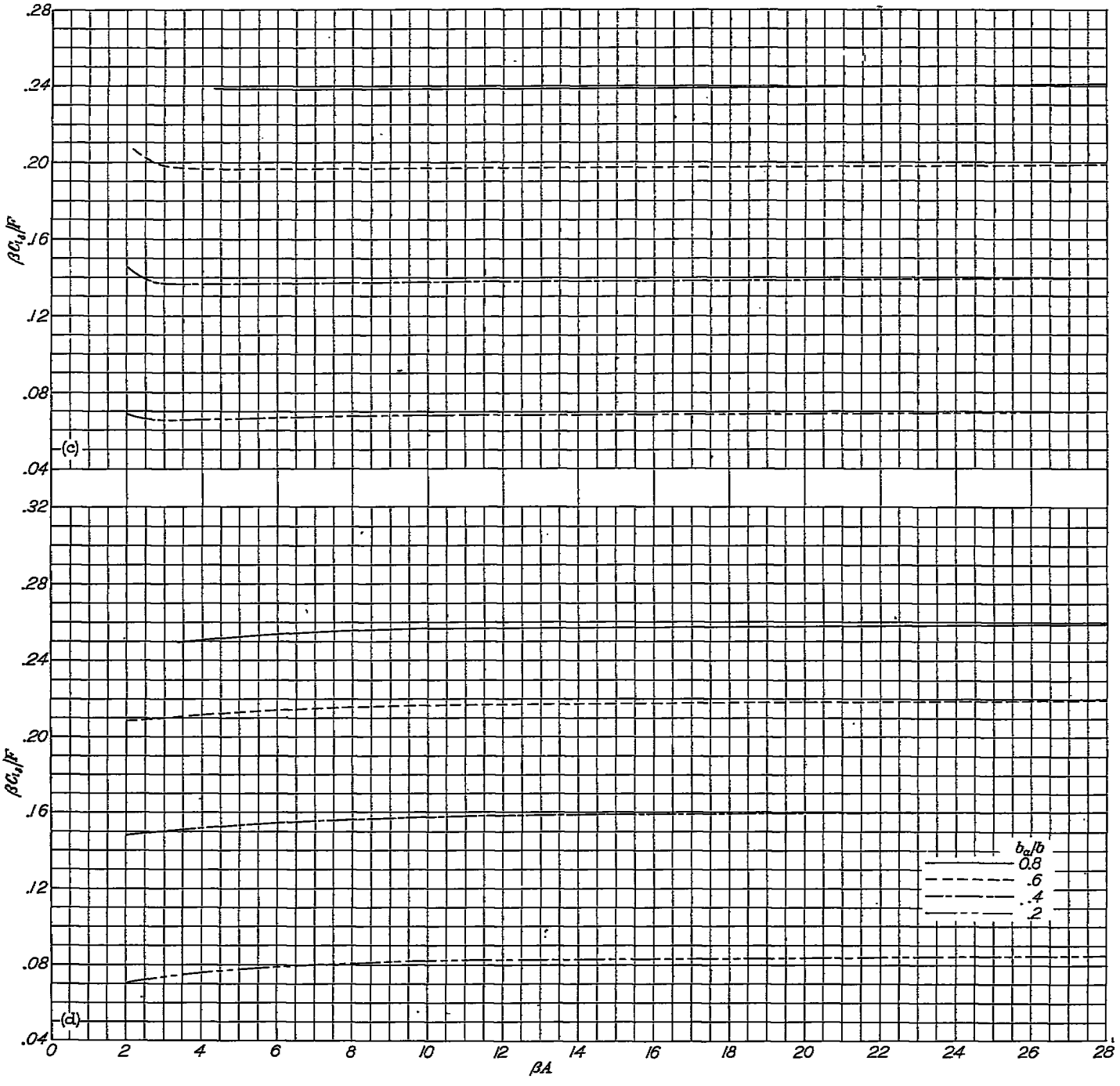

(c) $\lambda=0.4$.
(d) $\lambda=0.6$.

FIGURE 9.—Continued.

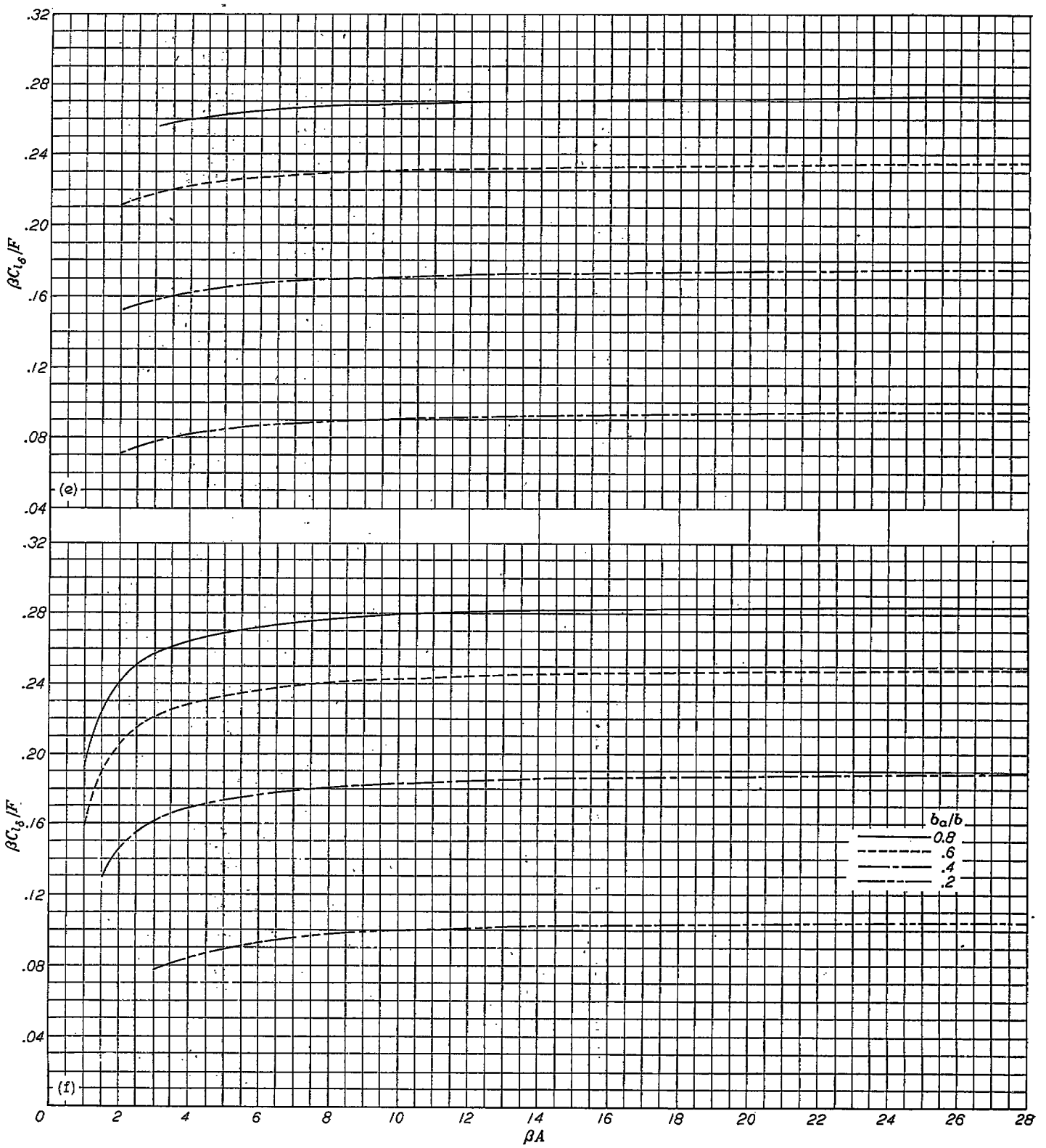

(e) $\lambda=0.8$.
(f) $\lambda=1.0$. (From reference 1.)

FIGURE 9.—Concluded.

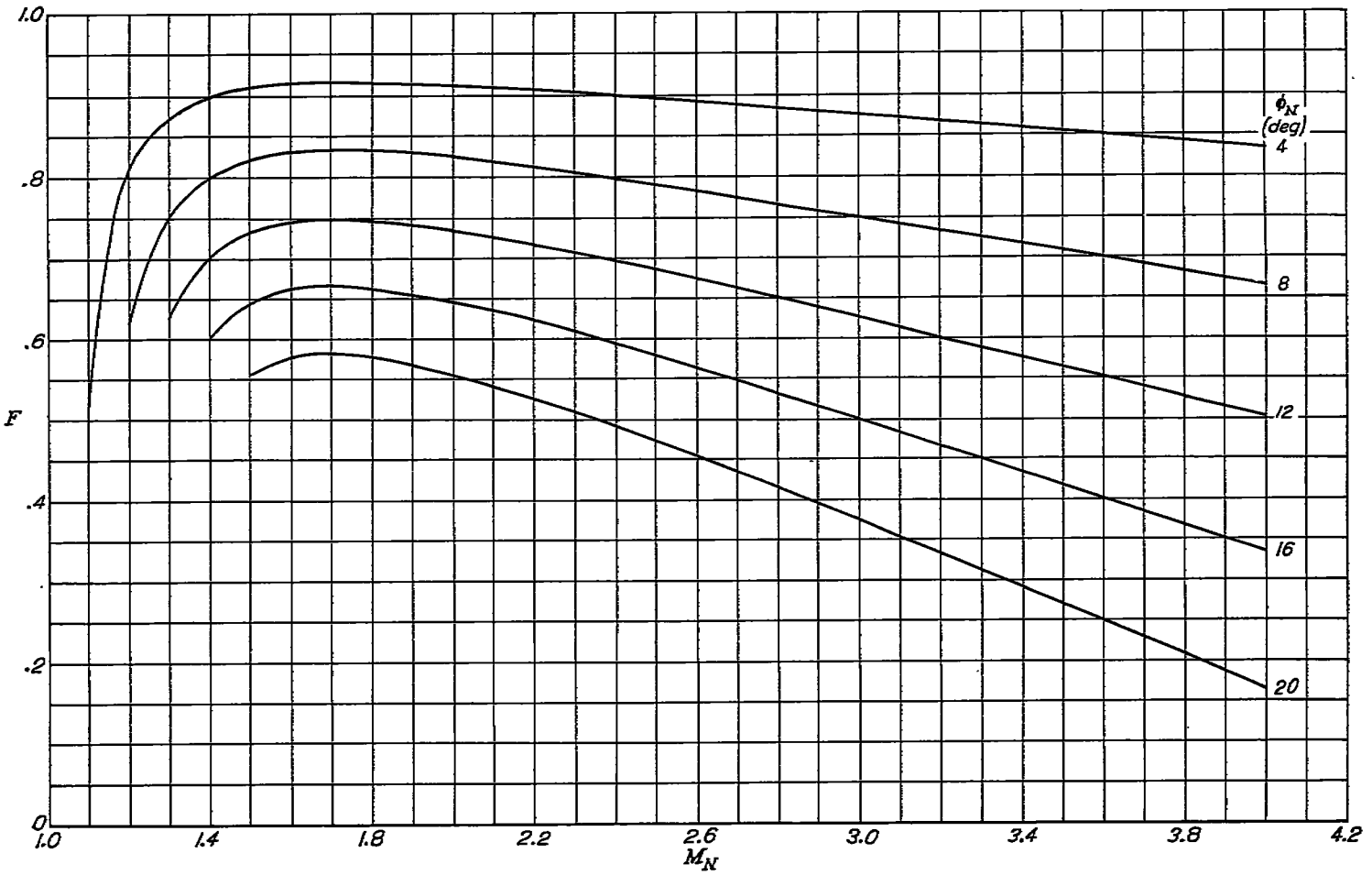

FIGURE 10.—Trailing-edge-angle reduction factor.

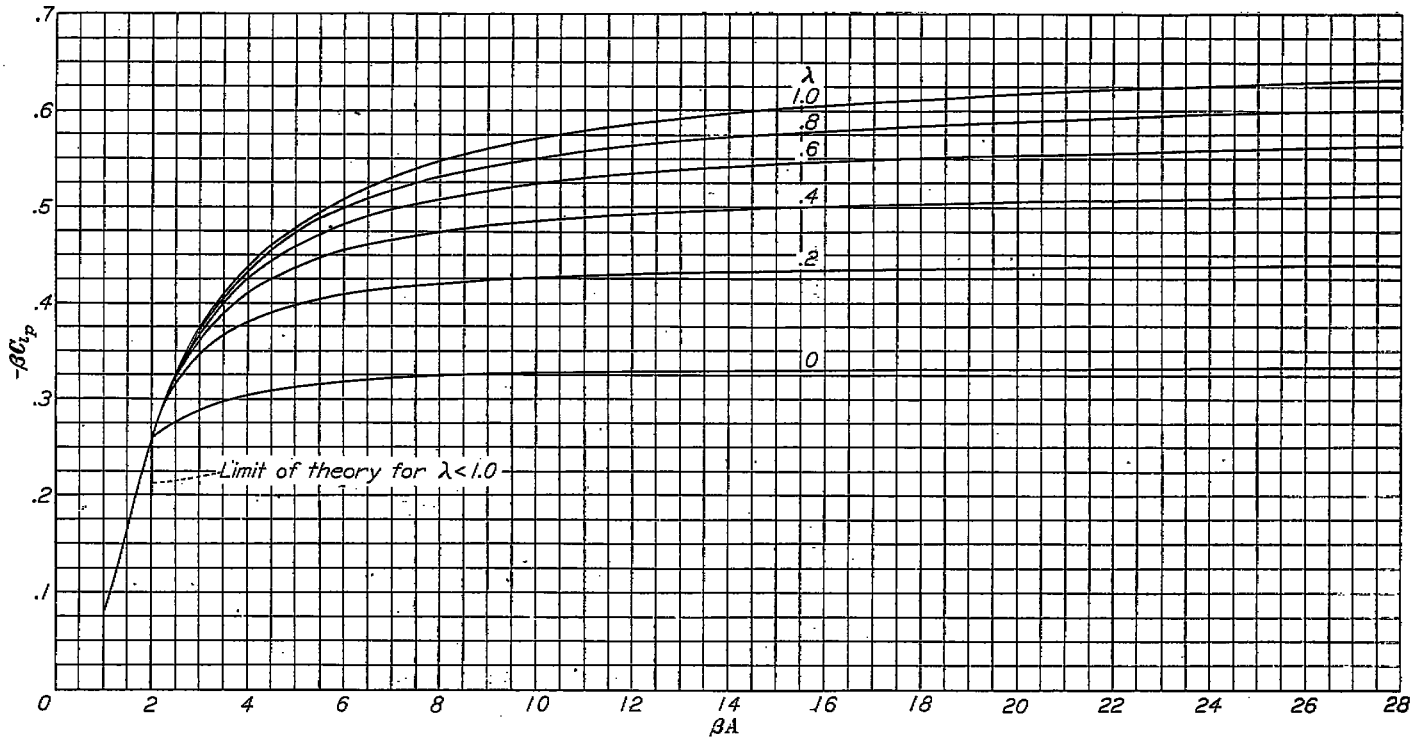

FIGURE 11.—Variation of damping-in-roll coefficient with βA. (From equation (21).)

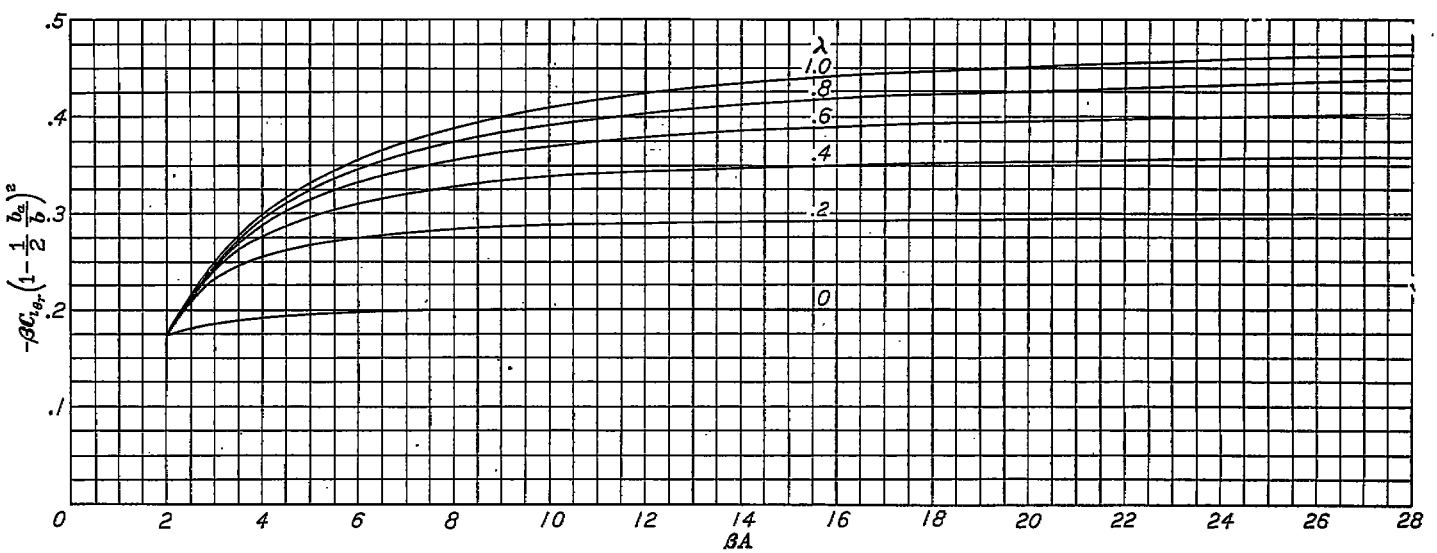

FIGURE 12.—Variation of rolling-moment-loss coefficient with βA. (From equation (23).)

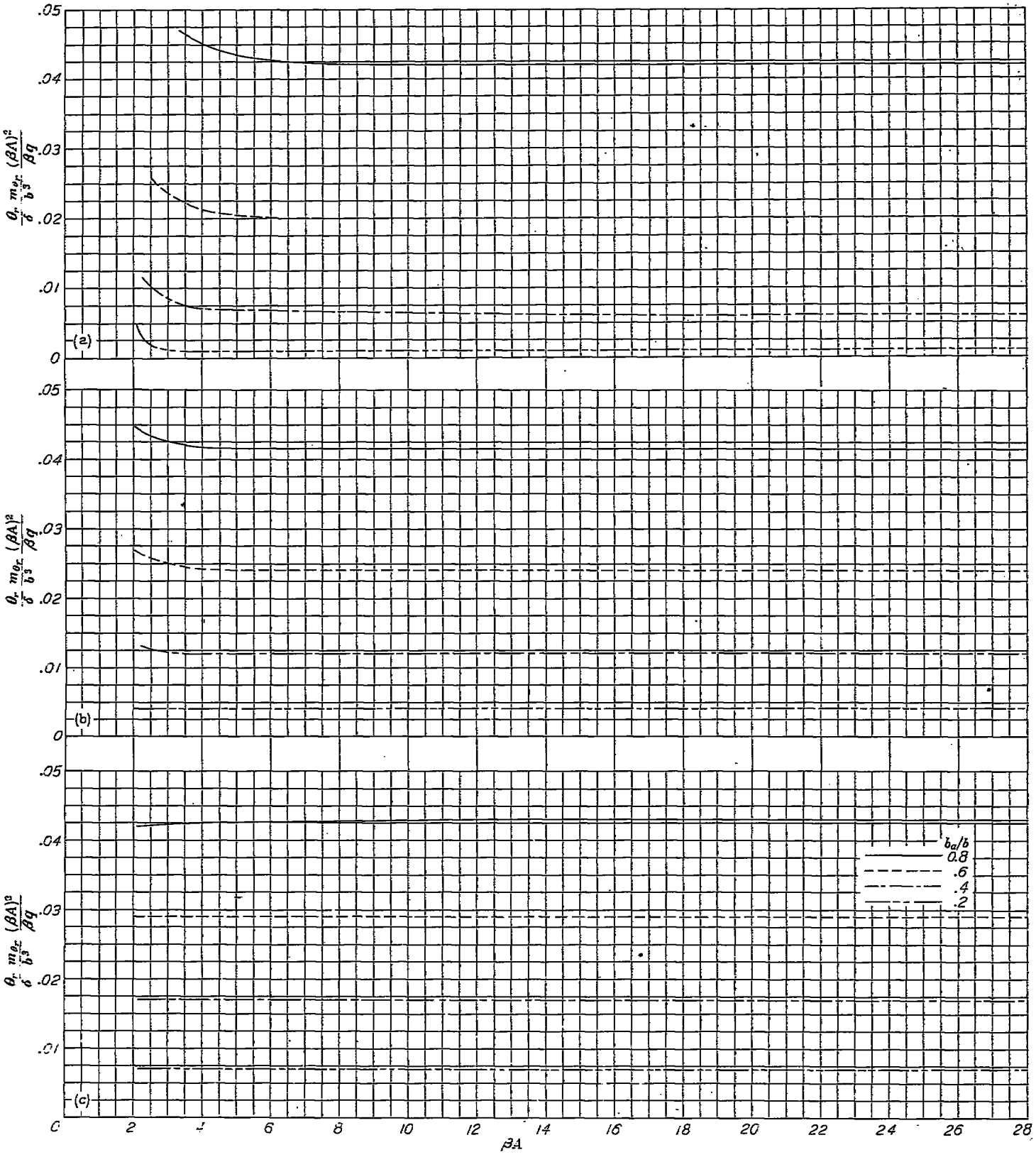

(a) $\lambda=0$.
(b) $\lambda=0.2$.
(c) $\lambda=0.4$.

FIGURE 13.—Variation of twist parameter with βA. $\frac{c_a}{c}=0.1$. (From equations (26).)

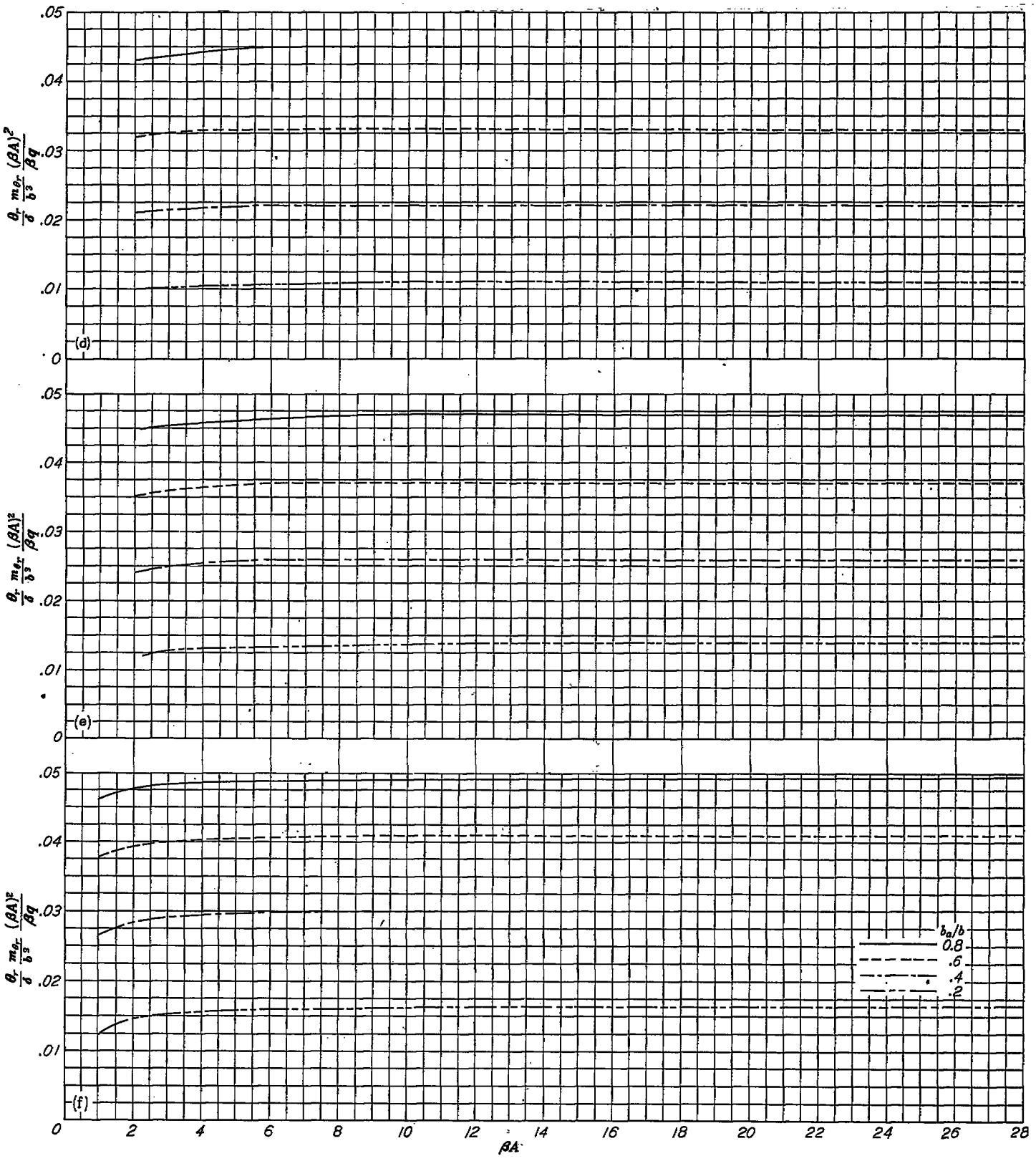

(d) λ=0.6.
(e) λ=0.8.
(f) λ=1.0. (From reference 1.)

FIGURE 13.—Concluded.

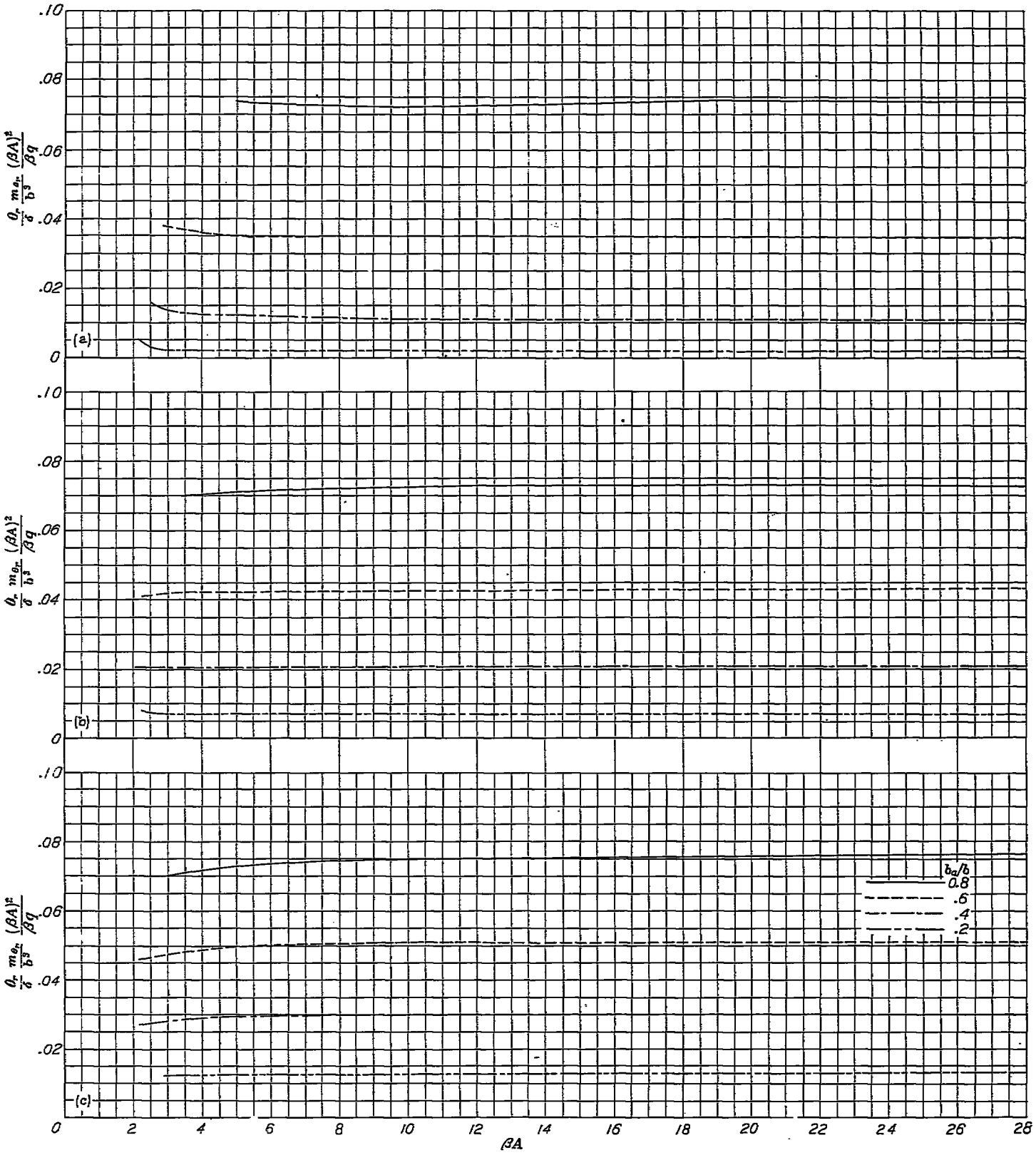

(a) $\lambda=0$.
(b) $\lambda=0.2$.
(c) $\lambda=0.4$.

FIGURE 14.—Variation of twist parameter with βA. $\frac{c_a}{c}=0.2$. (From equations (26).)

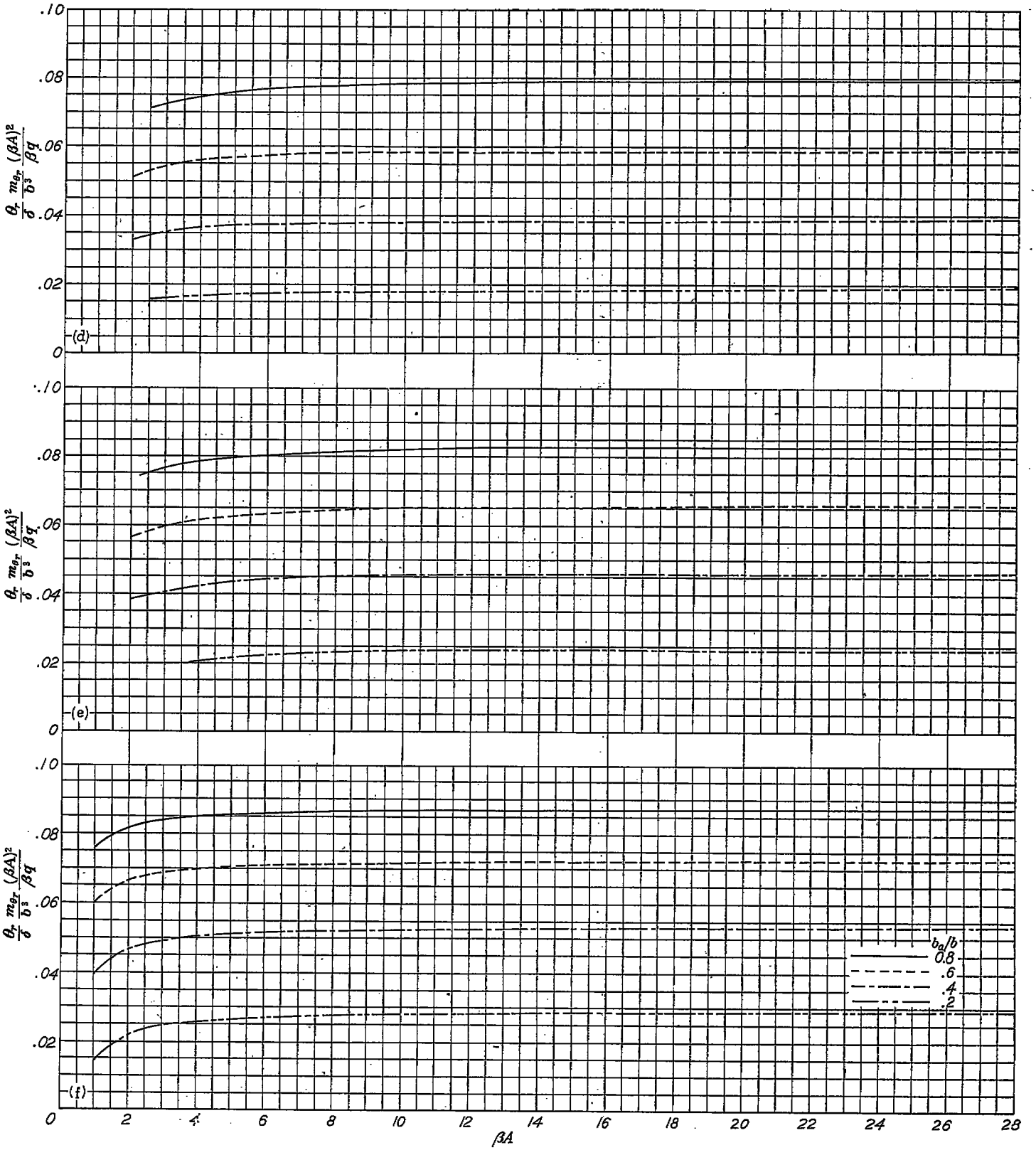

(d) λ=0.6.
(e) λ=0.8.
(f) λ=1.0. (From reference 1.)

FIGURE 14.—Concluded.

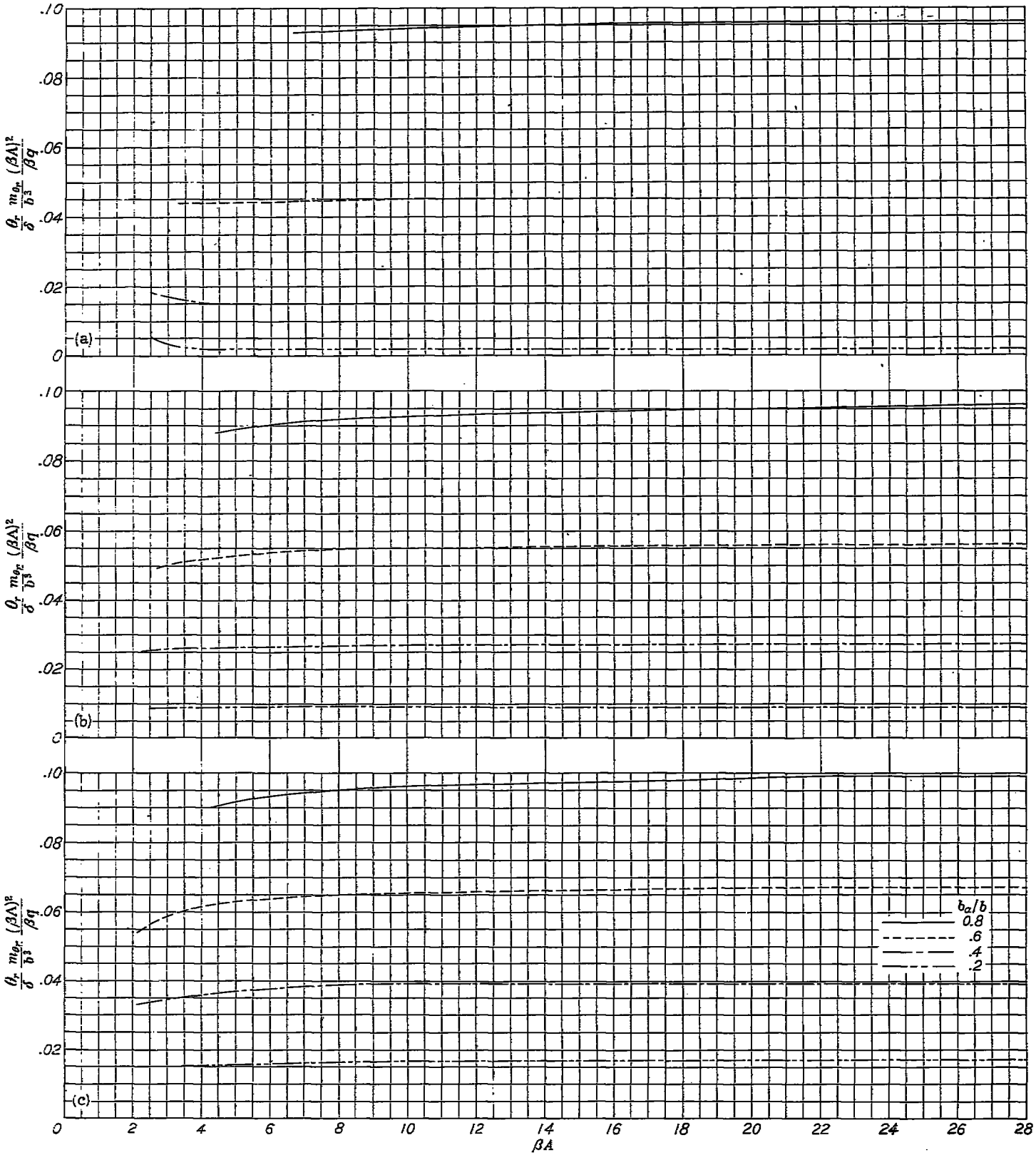

(a) $\lambda=0$.
(b) $\lambda=0.2$.
(c) $\lambda=0.4$.

FIGURE 15.—Variation of twist parameter with βA. $\frac{c_a}{c}=0.3$. (From equations (26).)

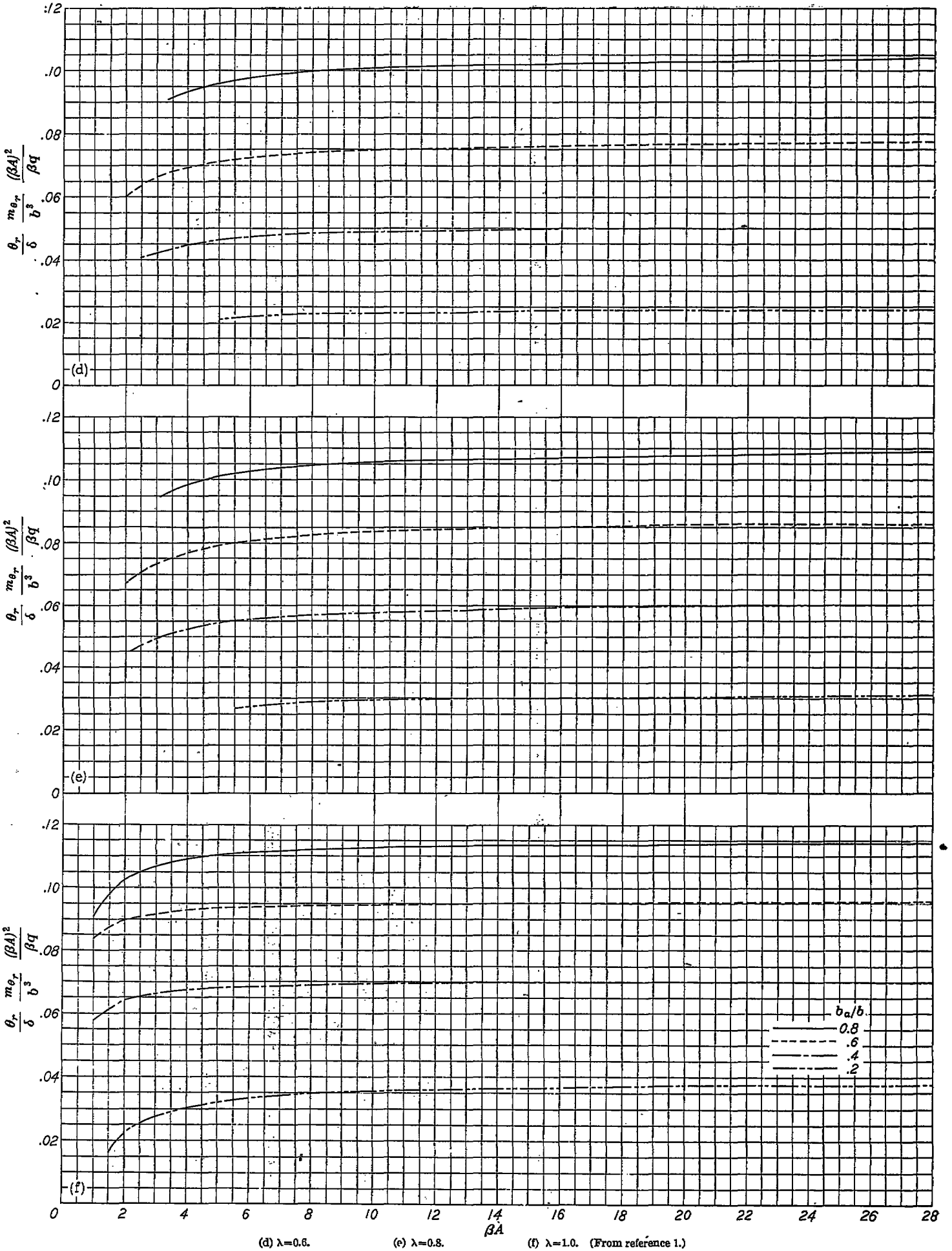

(d) λ=0.6. (e) λ=0.8. (f) λ=1.0. (From reference 1.)

FIGURE 15.—Concluded.

The aileron deflection δ used in βC_{l_δ} is measured in a plane parallel to the free stream. The value of the rolling-moment-effectiveness coefficient referred to an aileron deflection measured perpendicular to the hinge line can be obtained, if desired, by dividing βC_{l_δ} by the quantity $\sqrt{1+k_1^2}$.

The minimum value of βA for which each curve is plotted corresponds in most cases to the limit of applicability of the equation for the curve. Extrapolation of the curves is not recommended. The maximum value of b_a/b for which results are given is 0.8; this value is expected to lie close to the maximum that will be encountered on actual airplanes with fuselages.

The setup of table I can of course be altered. For example, a solution may sometimes be required for the torsional stiffness necessary to maintain a given percentage of the rate of roll that would be obtained with a perfectly rigid wing. In such a case, the solution can be obtained by recasting the last several columns, as shown in the table. If experimental data are available for any of the derivatives, these data may be used in place of the theoretical values of the present report.

Although an explicit solution for the reversal speed is impossible to obtain because of the complexity of the equations, the reversal speed is easily found by calculating the rate of roll through the speed range. The variation of the rate of roll with speed, however, is usually of more interest than the reversal speed alone; therefore, no extra calculations are involved in calculating the reversal speed.

The twist parameter θ_r/δ is directly proportional to q and inversely proportional to $m_{\theta r}$. (See equations (26).) Because of this relationship and because the other derivatives appearing in equations (2) and (3) are independent of q and $m_{\theta r}$, the values of $\frac{pb/2V}{\delta}$ and $\frac{pb/2V}{(pb/2V)_R}$ found from table I for specified values of altitude and stiffness are easily converted to values for other altitudes and degrees of stiffness.

Although the analysis was made by considering two wing panels lying in the same plane, experimental evidence exists which indicates that the results may with some justification be applied without change to configurations consisting of three or four wing panels, each containing an aileron, if the span and aspect ratio are taken as those of the wing formed by the reflection of a single panel. If the configuration consists of four panels, two of which contain ailerons, then the value of βC_{l_p} must be doubled.

The results of some calculations made for a hypothetical configuration are given in figure 16.

CONCLUDING REMARKS

An analysis has been presented of the effect of torsional flexibility on the rolling characteristics at supersonic speeds of tapered unswept wings with partial-span constant-percent-chord ailerons extending inboard from the wing tip.

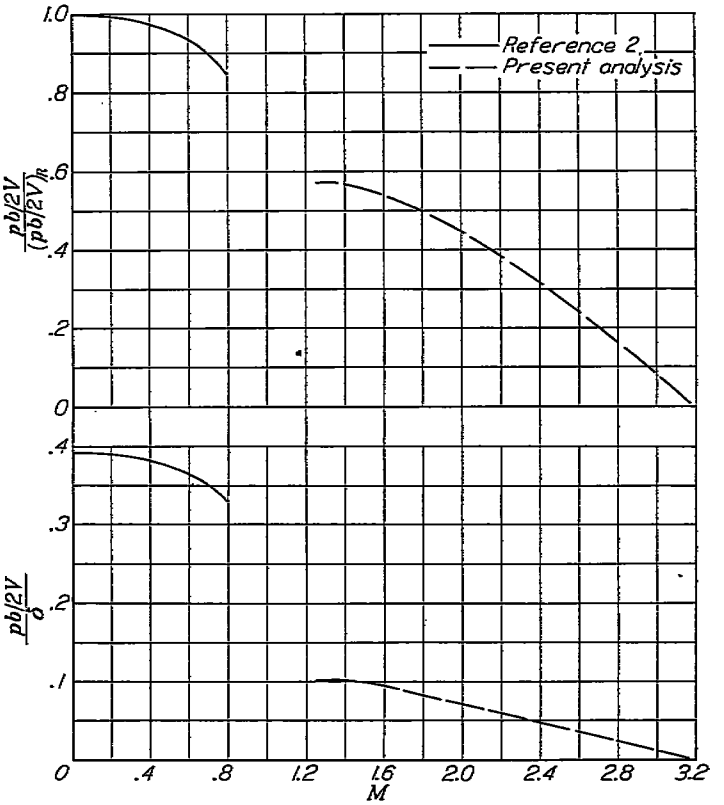

FIGURE 16.—Results of computations for a hypothetical configuration at sea level. $A=4$; $\lambda=0.4$; $\frac{b_a}{b}=0.4$; $\frac{c_a}{c}=0.2$; $b=30$ feet; $m_{\theta_r}=2{,}000{,}000$ foot-pounds per radian; $\phi_N=8°$.

Because of the complexity of the equations resulting from the analysis, numerical calculations were made from the equations and the results are presented in a series of figures. A computational form was prepared for use with the figures so that calculations could be made without reference to the analysis.

LANGLEY AERONAUTICAL LABORATORY,
NATIONAL ADVISORY COMMITTEE FOR AERONAUTICS,
LANGLEY FIELD, VA., *March 8, 1949.*

REFERENCES

1. Tucker, Warren A., and Nelson, Robert L.: The Flexible Rectangular Wing in Roll at Supersonic Flight Speeds. NACA TN 1769, 1948.
2. Pearson, Henry A., and Aiken, William S., Jr.: Charts for the Determination of Wing Torsional Stiffness Required for Specified Rolling Characteristics or Aileron Reversal Speed. NACA Rep 799, 1944.
3. Puckett, Allen E.: Supersonic Wave Drag of Thin Airfoils. Jour. Aero. Sci., vol. 13, no. 9, Sept. 1946, pp. 475–484.
4. Evvard, John C.: Distribution of Wave Drag and Lift in the Vicinity of Wing Tips at Supersonic Speeds. NACA TN 1382, 1947.

TABLE I

COMPUTATIONAL FORM

A=———— m_{θ_r}=———— ft-lb/radian

λ=———— b=———— ft

ϕ_N=———— deg (see equation (28))

$\frac{b_a}{b}$=———— $\frac{b^3}{m_{\theta_r}}$=————

$\sqrt{1+k_1^2}=\sqrt{1+\left(1-2\frac{c_a}{c}\right)^2\left(\frac{2}{A}\frac{1-\lambda}{1+\lambda}\right)^2}$=————

$\frac{c_a}{c}$=———— $\left(1-\frac{1}{2}\frac{b_a}{b}\right)^2$=————

①	②	③	④	⑤	⑥	⑦	⑧	⑨	⑩	⑪	⑫	⑬
βA	M	Altitude (ft)	$\beta q/(\beta q)_0$	$(\beta q)_0$	βq				$\frac{\beta C_{l_\delta}}{F}$	M_N	F	βC_{l_δ}
Assumed	Fig. 4		Fig. 5	Fig. 6	④×⑤	①^2	⑥/⑦	⑧×$\frac{b^3}{m_{\theta_r}}$	Fig. 7, 8, or 9	$\frac{②}{\sqrt{1+k_1^2}}$	Fig. 10	⑩×⑫

⑭	⑮	⑯	⑰	⑱	⑲	⑳	㉑	㉒	㉓
$-\beta C_{l_p}$	$-\beta C_{l_{\theta_r}}\left(1-\frac{1}{2}\frac{b_a}{b}\right)^2$	$-\beta C_{l_{\theta_r}}$	$\frac{\theta_r}{\delta}\frac{m_{\theta_r}(\beta A)^2}{b^3\beta q}$	θ_r/δ	$-\beta C_{l_{\theta_r}}\frac{\theta_r}{\delta}$			$\frac{pb/2V}{\delta}$	$\frac{pb/2V}{(pb/2V)_R}$
Fig. 11	Fig. 12	$\frac{⑮}{\left(1-\frac{1}{2}\frac{b_a}{b}\right)^2}$	Fig. 13, 14, or 15	⑰×⑨	⑯×⑱	⑬−⑲	⑲/⑬	⑳/⑭	1.0−㉑

Alternative arrangement for finding required torsional stiffness

⑱	⑲	⑳	㉑	㉒	㉓
$\frac{pb/2V}{(pb/2V)_R}$			θ_r/δ		m_{θ_r}
Assumed	1.0−⑱	⑬/⑯	⑲×⑳	$\frac{⑧\times⑰}{㉑}$	㉒×b^3